University of Stavanger

Faculty of Science and Technology

MASTER'S THESIS

Study program/ Specialization: Petroleum engineering / Reservoir engineering	Spring semester, 2011 Open access
Writer: Valery Dulov	…… (Writer's signature)
Faculty supervisor: Jann Rune Ursin External supervisor(s):	
Titel of thesis: Simulation of CO_2 injectivity in a laboratory cylindrical-cone model	
Credits (ECTS): 30	
Key words: Particle migration Dissolution of carbonates Change of permeability	Pages: 80 + enclosure: …… Stavanger, 09.06.2011 Date/year

Abstract

In this thesis the processes (caused by injection of carbon dioxide) - mainly migration of particles and dissolution and precipitation of carbonates - which cause changing of permeability (and consequently injectivity) are studied.

In chapter 2 we study previous investigations and theories, made by different researchers and related to our topic. The goal of this chapter is to sum up all previous researches and to understand the physical processes in reservoir during the injection of CO_2.

Chapter 3 is mainly dedicated to creating of a mathematical model of particle migration. Main formulas for the model is presented and described there. Also chapter contains description of a program (on MatLab), where this mathematical model is implemented.

Chapter 4 deals with the description of physical (cylindrical-cone) model (which does not exist now, but will be constructed in nearest future) and with computer simulation (in CMG Stars). The result of simulation is the changing of pressure distribution in reservoir (including changing of pressure near the injection well – changing of injectivity), caused by particle migration due to injection of carbon dioxide.

Thus, the main result of this work is the computer program, where all the theoretical investigations are implemented, and simulation, based on the data, produced by this program.

List of figures

TABLE OF CONTENTS

1 INTRODUCTION

Emission of carbon dioxide (and other green-house gases) into atmosphere is the one of the most important ecologic problems nowadays. One of the ways to decrease CO_2-emition is a sequestration of carbon dioxide in aquifers.

Processes, which occur in reservoirs during injection of CO_2, are still under investigation. There were number of experiments – both core-scale and field-scale – which study processes in rocks during injection of carbon dioxide. Most of them show quite opposite results. While in the most of core-flooding experiments [6], [16] permeability (and consequently injectivity) increases, field-scale experiments [3] show decreasing of permeability. It looks like contradiction, but actually it is not. Fore core experiments they use relatively short core samples (rarely longer than 30 cm) and main process there is dissolution of calcium carbonate and mobilization of particles, while processes of retention of carbonates and particles (mainly due to decreasing of velocity of flow) are not observed.

Therefore, porosity and permeability are likely to significantly decrease further away from the well-bore, caused by fines migration and adhesion, - a process not cached in core flooding tests [17].

Because of this, experimental setup, larger than core and smaller than field, is needed. Gas group at the Department of petroleum engineering, University of Stavanger has proposed such an experimental setup. The proposed experiment is scaled according to pressure gradients observed in field injection studies. Radial geometry is preserved and scaled in the laboratory experimental setup. The model will be filled with a porous medium, made up of unconsolidated rock material: minerals of silica, calcite and other rock fragments. Two mechanical models have been examined: cake-slice model and cylindrical-cone model.

Objectives of the project:

1. To understand the mechanisms, which cause injectivity decline during injection of carbon dioxide;

2. To develop mathematical model of these processes and design a program for calculation of changing of main properties, such as porosity and permeability;

3. To perform a simulation in CMG Stars with new changing properties.

As long as experimental setup does not yet exist, this work is rather theoretical and a lot of assumptions for developing mathematical model and performing a simulation present. However, after setup will be ready for conducting the experiments, it will be fairly easy to implement actual experimental data instead of assumptions.

2 THEORETICAL BACKGROUNDS

There are a significant amount of researches and theories dealing with formation damage in reservoir caused by injection of different liquids. Our task here is to define processes, which deals with injection of carbon dioxide and its consequences. In this chapter we are trying to sum up all the previous researches (which we have studied) into the theory, which describes, as fully as possible, processes caused by injection of CO_2 and its interacting with reservoir.

2.1 Sequestration of CO_2

Over the last century the global average temperature has increased by 0,6°C, ice extent has reduced considerably, the sea level has risen. Scientists are pretty sure that all of these problems were caused by the emission of anthropogenic greenhouse gases (mainly CO_2) into the atmosphere. More than 13 Gig tons of carbon dioxide is emitted every year, of which more than 70% comes from burning fossil fuels [15].

Carbone capture and storage could play a major role in reducing greenhouse gas emission to the atmosphere. Carbone capture and storage includes separation of CO_2 from industrial and energy-related sources, transport and storage of carbon dioxide.

For the time being CO_2 mostly has been used in petroleum industry as one of the methods of enhance oil recovery, and this knowledge and experience could be used to design save storage in other subsurface settings. Already in several commercial and pilot projects (Sleipner Vest [1]) geological sequestration of carbon dioxide in oil and gas reservoirs, aquifers and coal beds is currently being tested.

Geological sequestration implies that carbon dioxide must be trapped in reservoir without any possibility to escape. Trapping mechanisms are any chemical or physical processes through which CO_2 can be stored in geological environment such that it is unlikely to escape. The efficiency of long-term storage in aquifers will be directly related to the efficiency of each of the trapping mechanisms involved.

There are four major trapping mechanisms for carbon dioxide storage in aquifers [15]:

1. Hydrodynamic (structural or stratigraphic) trapping, where cap rock prevents CO_2 from flowing back to the surface;

2. Residual or capillary trapping, where capillary forces and relative permeability effects will contribute to converting the CO_2 injected into immobile phase;

3. Solubility trapping, where CO_2 dissolves in aqueous phase;

4. Mineral trapping, where chemical reactions between CO_2 and rock minerals forms a solid carbonate.

Injection of CO_2 into aquifers includes numerous of physical and chemical processes [10]:

1) multiphase flow;

2) dissolution-deposition kinetics;

3) solute transport;

4) hydrodynamic instabilities due to displacement of less viscous brine with more viscous carbon dioxide (viscous fingering);

5) capillary effects and upward movement of CO_2 due to gravity (gravity override).

Reactions between the formation rock, the aquifer fluid and carbon dioxide may lead to change in the formation permeability and the effective porosity, thus lead to formation damage in reservoir and decreasing of injectivity.

2.2 Formation damage

Formation damage is undesirable reduction of permeability by various processes occurring in geological porous formations and therefore reducing the productivity and injectivity of the wells.

In our case two kinds of processes can be the cause of formation damage:

1) Chemical processes - redistribution of carbonate material in porous media (dissolution, transport and precipitation of carbonate);

2) Mechanical processes - redistribution of particles in porous media (mobilization, transport and retention of particles).

2.3 Chemical processes

Carbon dioxide in reservoir will form a carbonic acid, which will react with reservoir minerals. In a formation reach with carbonate material major cause of reductions in rock properties is precipitation of calcium bicarbonate.

2.3.1 Chemical processes in reservoir

1) Gas dissolution

$$CO_2 \leftrightarrow CO_{2\,aq}; \tag{2.1}$$

2) Carbonic acid formation

$$CO_{2\,aq} + H_2O \leftrightarrow H_2CO_{3\,aq}; \tag{2.2}$$

3) Carbonic acid equilibrium

$$H_2CO_{3\,aq} \leftrightarrow H^+_{aq} + HCO^-_{3\,aq}, \tag{2.3}$$

$$HCO^-_{3\,aq} \leftrightarrow H^+_{aq} + CO^{2-}_{3\,aq}; \tag{2.4}$$

4) Calcium carbonate dissolution

$$CaCO_{3\,s} + H_2CO_{3\,aq} \leftrightarrow Ca^{2+}_{aq} + 2HCO^{-}_{3\,aq}, \quad (2.5)$$

$$CaCO_{3\,s} + H^{+}_{aq} \leftrightarrow Ca^{2+}_{aq} + HCO^{-}_{3\,aq}, \quad (2.6)$$

here s – in solid phase,

aq – in aqueous phase.

Figure 2.1 shows us that on the wide range of pH HCO_3^--ions prevail over carbonic acid and CO_3^{2-}-ions, it means that calcium carbonate is likely to be dissolute and calcium bicarbonate to be formed.

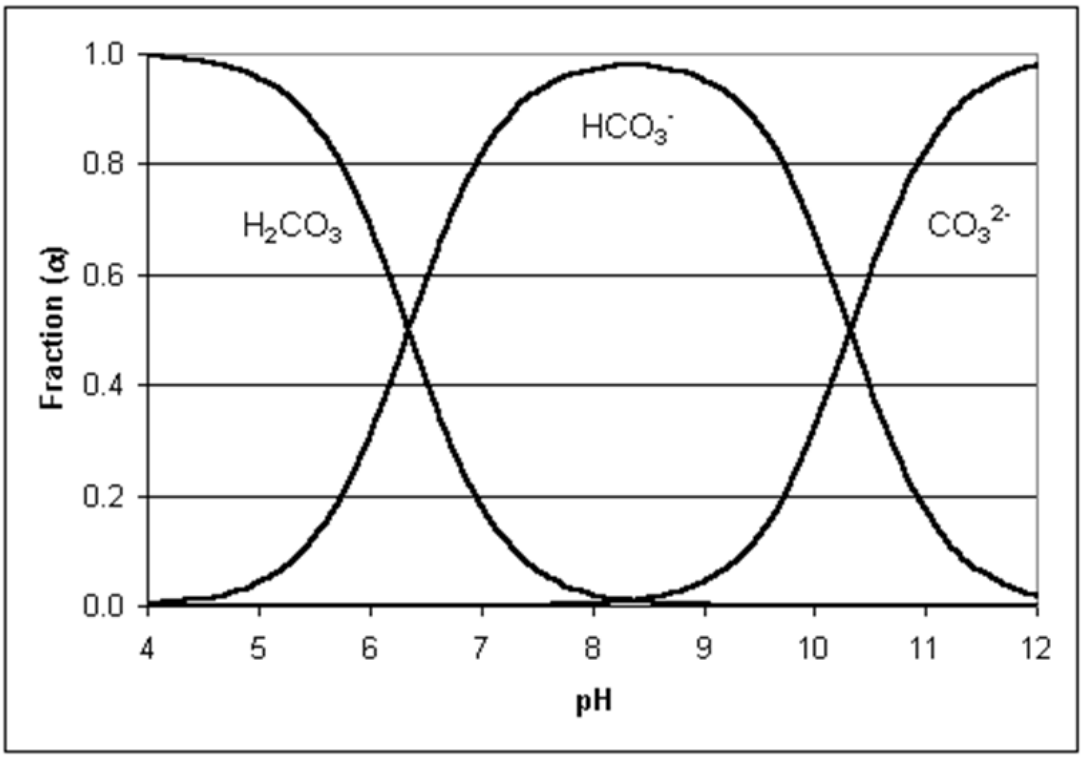

Figure 2.1 - The pH-dependent fractions [18]

2.3.2 Dimensionless numbers

These processes mainly governed by Peclet and Damkohler numbers.

The Peclet number is defined as the ratio of transport by convection to transport by dissolution:

$$Pe = \frac{Ud}{D} \tag{2.7}$$

where U is velocity,

d is characteristic distance,

D is particle diffusion coefficient.

The Damkohler number is defined as the ratio of the net rate of dissolution by acid to the rate of convective transport of acid. When the rate of reaction is very rapid compared to the rate of mass transfer, the net rate of dissolution is mass transfer limited and the Damkohler number is given by

$$Da_m = \frac{aD_e^{\frac{2}{3}}L}{Q}, \tag{2.8}$$

where D_e is the effective diffusion coefficient,

Q is the flow rate,

L is the pore length,

a is the constant that depends on the carbonate sample.

When the rate of reaction is very slow compared to the rate of mass transfer, the net rate of dissolution is reaction rate limited and Damkohler number is given by

$$Da_r = \frac{ak_rDL}{Q}, \tag{2.9}$$

where k_r is the surface reaction rate constant,

D is the pore diameter.

Dissolution behavior [10]:

1. High Pe and PeDa numbers: wormholes are formed and permeability increases greatly due to the dissolution process.

2. Low Pe and high PeDa numbers: reactions mainly occur at the inlet boundary, resulting in the face dissolution and the slowest increase of the permeability in the dissolution process.

3. Moderate Pe and PeDa numbers: reactions are generally non-uniform, with more in the upstream and less in the downstream.

4. Very small PeDa number: dissolution or precipitation is highly uniform, and these two processes can be approximately reversed by each other.

2.4 Mechanical processes

After dissolution of calcium carbonate (which is likely to function as cement for fine rock particles) occurs, particles can easily migrate (forced by flow of carbon dioxide) through porous media and be redeposited further on. Therefore it is important to know mechanisms of these processes and forces which influence them.

2.4.1 Source of particles

Most of sands and sandstones contain clays and other fine particulate matter. Depending on their origin two different types of clays are distinguished [14]:

1. Detrital clays which have sedimented with the sand grains at the time the bed was deposited;

2. Diagenetic clays which have subsequently precipitated from formation waters or were formed by the interaction of formation waters with pre-existing clay minerals.

Detrital clays mostly form an integral part of the overburden supporting rock matrix and therefore are not mobile. On the other hand, diagenetic clays are usually

deposited on pore walls, they do not support the overburden pressure and can move without causing disaggregation of the rock matrix. Such clays are likely to be mobilized under certain conditions and can be cause of fines migration in porous media with associated permeability and injectivity reduction. There can be other mechanism of permeability reduction, like swelling clays, but it is now commonly accepted that fines migration in the form of clays or other fine particles is the major mechanism for permeability decline.

2.4.2 Mobilization of particles

The factors contributing to clay particle expansion and dispersion [7]:

- hydration of exchangeable cations;
- hydration of particle surfaces;
- repulsion of interacting atmospheres of exchangeable cations (double layer theory);
- desorption of chemical removal of sorbed binding matter;
- neutralization of positive charges on particle edges;
- mechanical shear;
- thermal (Brownian) motion.

All of these mechanisms and some others contribute to particle mobilization, but the main factor for particle to be suspended into porous fluid is velocity of this fluid. Gruesbeck and Collins [8] have investigated that there is a critical velocity above which the permeability was a linearly decreasing function of the fluid velocity (figure 2.2), meaning the larger the velocity the more particles is redistributed, while below critical velocity permeability reduction was not observed, meaning particles almost were not suspended into reservoir fluid. Critical velocity depends on properties of porous media and contained fluids.

In our case also dissolution of carbonates plays a significant role. After dissolution of carbonates significant amount of clay which was entrapped by carbonate cement could be easily suspended.

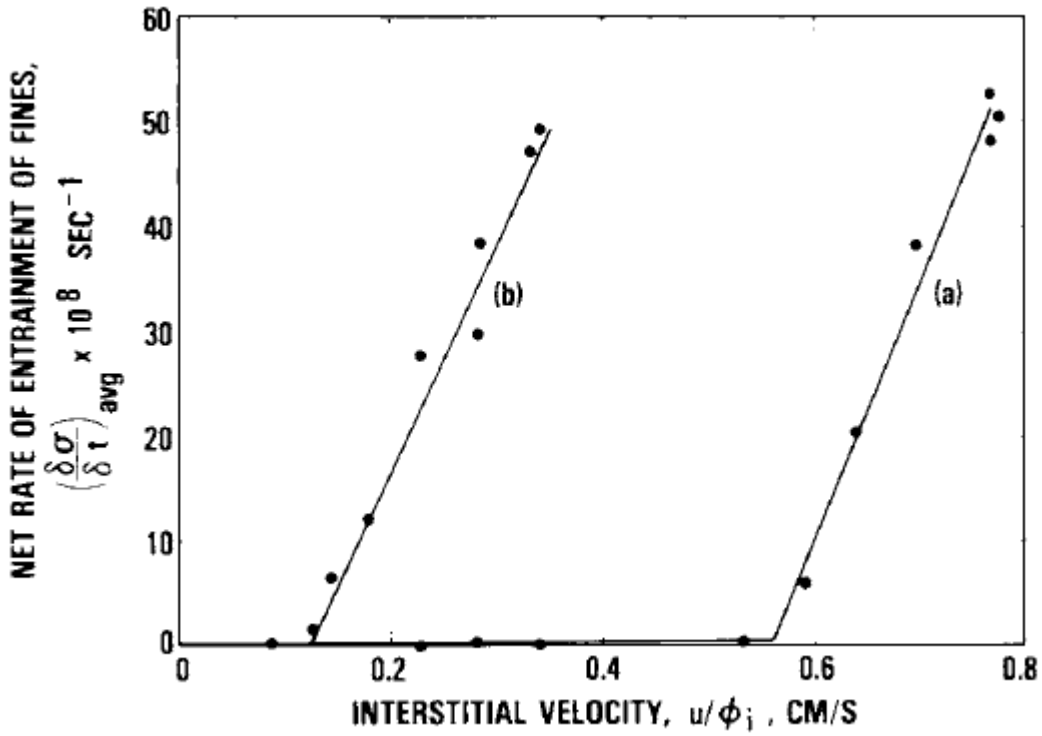

Figure 2.2 – Net rate of entrainment of fines in a porous medium:

a) fluid viscosity 1 mPa·s; b) fluid viscosity 10 mPa·s [8]

2.4.3 Retention of particles

Researches [4] have shown that 4 phases (figure 2.3) occur during deposition of particles:

1. Surface deposition;
2. Pore bridging;
3. Internal cake formation;
4. External cake formation.

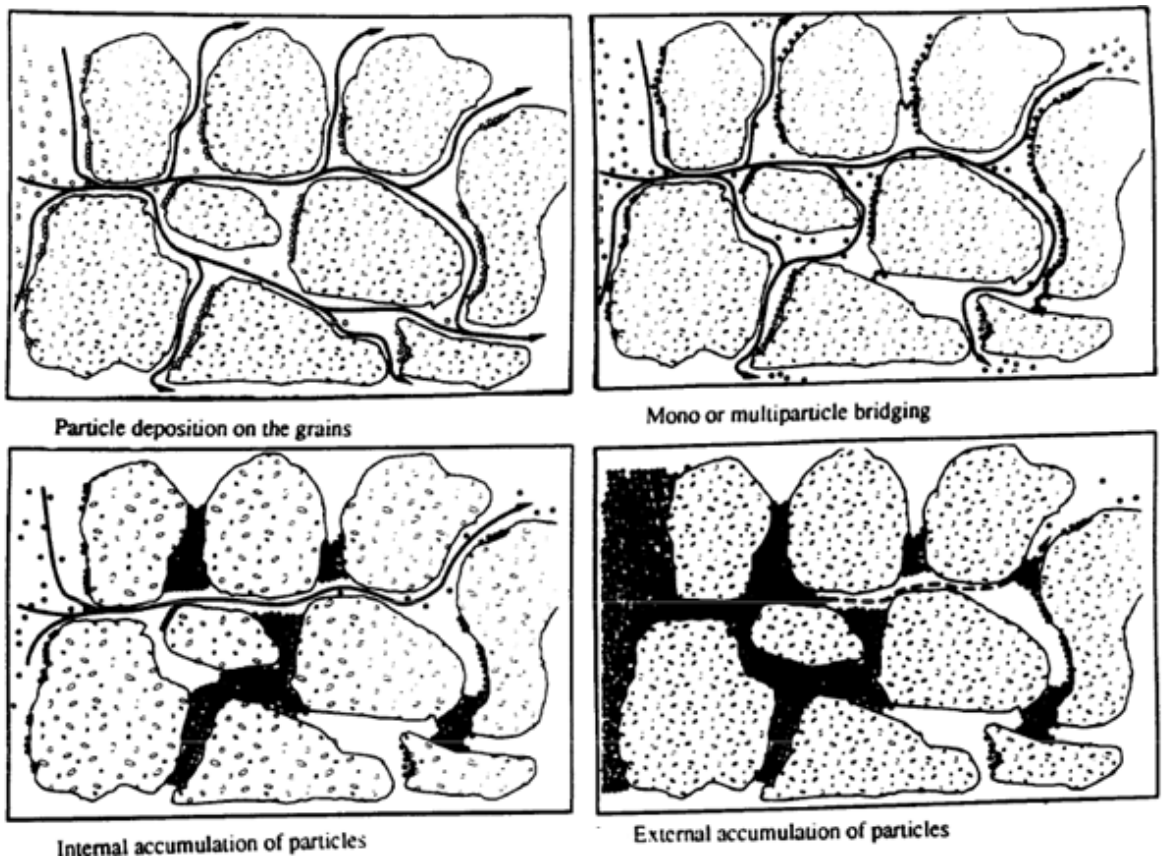

Figure 2.3 - Phases of deposition of particles [12]

2.4.3.1 Surface deposition

In this phase particles deposit onto grain/pore surface.

In general the main factors contributing to deposition of particles on the pore walls are [7]:

- van der Waals forces;
- recrystallization and chemical alteration;
- sorption of organic matter from oil;
- mutual sorption of ions between adjacent unit layers;
- electrostatic attractions between positively charged edges and negatively charged faces;

- the thermodynamic drive to reduce interfacial free energy by reducing surface area.

Some of these forces is shown on figure 2.4.

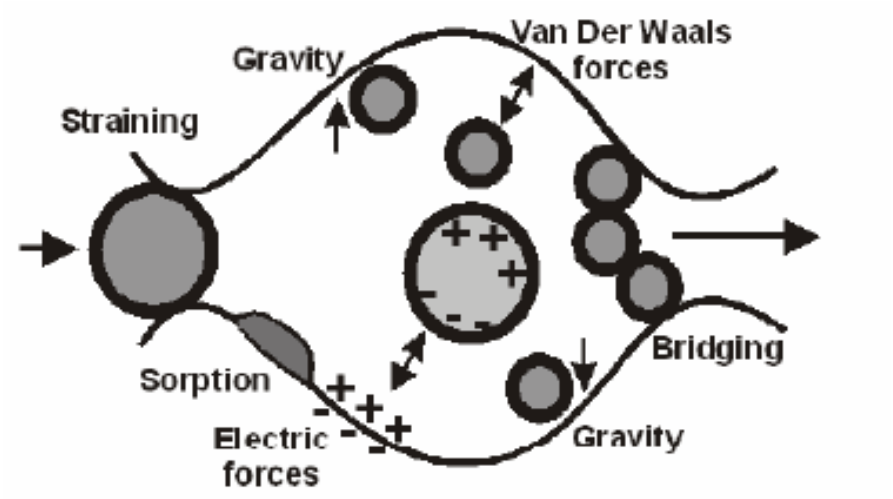

Figure 2.4 - Capture mechanisms of solid and liquid particles [9]

The kinetics of surface deposition is flow direction increases. The effect of particle deposition on permeability is significant only if it takes place in pore throats, i.e. for θ close to $\pi/2$ (figure 2.5). Thus reduction of permeability is mainly not related to the total amount of deposited particles but only to the fraction deposited in the pore throat area. However additional viscous forces (which depend on the particle-to-grain size ratio and pore structure) created around the deposited particles may contribute to permeability reduction.

When the energy barrier opposing aggregation is not very high, multilayer deposition can occur during this surface deposition phase.

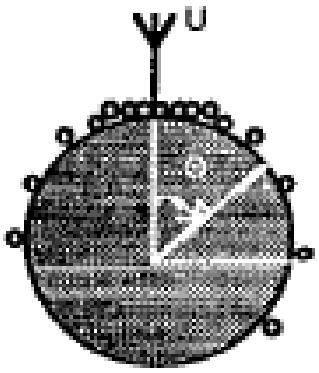

Figure 2.5 - Deposition of particles relative to the direction of flow [4]

Surface deposition regimes [4]

1. Pure diffusion regime: diffusion forces dominate convection for the transport of particles to the grain surface, which means very slow flows or very small particles, therefore has a negligible practical importance for formation damage.

2. Convective-diffusion regime: in this regime Peclet number is much larger than 1. Peclet number can be defined as the convection to diffusion forces ratio. When particle/collector interactions are attractive or weakly repulsive, all diffusing particles reaching the grain are deposited.
When the grain surface is partially covered by already deposited particles, the deposition probability on the surface area located downstream from deposited particles is decreased by so-called hydrodynamic shadowing effect. Consequently the deposition rate in pore throats, which determines the rate of permeability decrease, is reduced by hydrodynamic shadowing.

3. Hydrodynamic regime: here hydrodynamic forces play a significant role in the deposition either by reducing the energy barrier between particle and grain surface or by enhancing the escape probability.

4. The interception regime: at very high Peclet numbers the deposition flux becomes independent of the surface force and proportional to Peclet number.

2.4.3.2 Pore bridging

In this phase particles are convected towards a region of pore space (e.g. pore throat) where the gaps between two or three grains are smaller than its size (figure 2.6). There particles are trapped either hydrodynamically (i.e. unable to diffuse backwards to escape) in case of repulsive forces between particles and grains or by surface forces in attractive case.

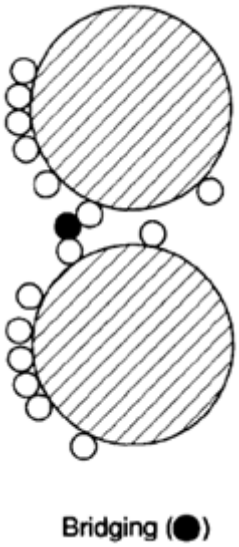

Figure 2.6 - Pore bridging [11]

Particles may be attached either to two particles already deposited onto pore throat surface (three-particle bridging) or to a previously deposited particle and pore throat surface (two-particle bridging).

Types of pore bridging [4]:

1) Mono-particle bridging: deposition of one particle forming a bridge by having two contact points with the pore wall (case when particles are larger than pore throat) or two contacts with previously deposited particles.

2) Multi-particle bridging: several particles arrive at the same time to the pore throat to form a bridge.

3) Bridging by multilayer deposition: for weakly repulsive particles, multilayer formation can lead to bridging.

2.4.3.3 Internal cake formation

When the fraction of bridged pores reaches a critical value, the pores are no longer connected over some critical characteristic depth (damage depth). At this point particles start to accumulate not only upstream from bridged pore throats but also inside pore bodies (which are still accessible), forming what is conventionally called internal cake.

2.4.3.4 External cake building

Accumulation of particles upstream from the inlet of porous medium (not present in our case).

3 MATHEMATICAL MODEL

This chapter is dedicated to implementation of theories (studied in chapter 2) into mathematical model. The main result is the computer program (which could be found in appendix A), which is based on the formulas and algorithms described here. This program calculates changes in permeabilities and porosities taking into account the processes, which occur during injection of carbon dioxide into reservoir.

And as in previous chapter our main concerns are:

1) chemical processes, related to dissolution and precipitation of calcium carbonate and

2) mechanical processes, related to redistribution of particles.

3.1 Dissolution of calcium carbonate

Dissolution of calcium carbonate is a chemical process described with methods and equations of physical chemistry.

3.1.1 Rate of reaction

The reaction rate describes whether reaction is slow or fast.

Conceder a typical reaction:

$$aA+bB=cC+dD, \tag{3.1}$$

where a, b, c, d – stoichiometric coefficients,

A, B – reactants,

C, D – products.

Then rate of reaction is defined as

$$r = -\frac{1}{a}\frac{d[A]}{dt} = -\frac{1}{b}\frac{d[B]}{dt} = \frac{1}{c}\frac{d[C]}{dt} = \frac{1}{d}\frac{d[D]}{dt}, \tag{3.2}$$

where [X] denotes the concentration of the substance X (X stands for A, B, C and D).

Also reaction rate could be expressed as

$$r = k(T)[A]^a[B]^b, \tag{3.3}$$

where k(T) is the reaction rate coefficient or rate constant, although it is not really a constant, because it includes all the parameters that affect reaction rate, except for concentration, which is explicitly taken into account.

3.1.2 Temperature dependence

The temperature is the most important parameter which affects the reaction rate coefficient. A temperature dependency could be found from Arrhenius equation:

$$k = k_0 e^{\frac{-E_a}{RT}}, \tag{3.4}$$

where R – the gas constant,

E_a – activation energy, which could be found experimentally:

$$E_a = \frac{2.3Rln\left(\frac{k_{T2}}{k_{T1}}\right)T_1T}{T_2 - T_1}, \tag{3.5}$$

where k_{T1} and k_{T2} are the experimentally obtained reaction rate coefficients for temperatures T_1 and T_2 correspondingly.

The easier way to estimate temperature dependency on reaction rate is to use empirical Vant-Hoff's rule: "with increasing temperature for every 10 degrees the rate constant for homogeneous elementary reaction increases in two - four times", which could be expressed as an equation as

$$r_2 = r_1\gamma^{\frac{T_2 - T_1}{10}}, \tag{3.6}$$

where γ – constant, γ∈[2;4].

But Vant-Hoff's rule has some restrictions; it could not be applied for high temperature reactions, for very slow or very fast reactions.

3.1.3 Reversible reactions

For reversible reactions:

$$r = r_1 - r_2 = k_1[A]^a[B]^b - k_2[C]^c[D]^d, \quad (3.7)$$

where r_1 – rate of forward reaction,

r_2 – rate of backward reaction.

As we can see rate of reversible reaction depends on concentration of reactants and products of reaction. As long as (in our case) concentration of reactants is approximately constant and high, rate of reaction depends on concentration of products. Concentration of products depends on velocity of fluid in reservoir and could be described by Peclet and Damkohler numbers (see 2.3.2).

3.1.4 Rate of dissolution of calcium carbonate

Now we should connect rate of reaction with volume of calcium bicarbonate which came into solution. For this purpose we can use dimension analysis.

Dimension of the reaction rate is

$$[r] = \frac{mol}{s \cdot m_{sol}^3}. \quad (3.8)$$

We can multiply reaction rate by molar mass and divide by density of calcium carbonate:

$$\left[\frac{r \cdot M}{\rho}\right] = \frac{mol}{s \cdot m_{sol}^3} \frac{kg}{mol} \frac{m_{CaCO_3}^3}{kg} = \frac{m_{CaCO_3}^3}{s \cdot m_{sol}^3}. \quad (3.9)$$

Volume of solution is equal to pore volume. So, rate of dissolution of calcium carbonate (expressed in cubic meters per second) in volume V of rock is:

$$r_{CaCO_3} = \frac{r \cdot M \cdot V_{rock} \cdot \varphi}{\rho}. \quad (3.10)$$

Value of new porosity after dissolution:

$$\varphi_1 = \frac{V_{rock} \cdot \varphi + r_{CaCO_3} \cdot t}{V_{rock}}, \quad (3.11)$$

where t – time of interest.

3.1.5 Algorithm for finding of rate of dissolution of calcium carbonate

Now we should sum up the information above into algorithm:

1. The reaction rate coefficients (k) should be obtained from experiment.

2. Influence of reservoir temperature should be considered by using either Arrhenius equation (activation energy should be calculated according to experiment's data) or Vant Hoff's rule (only if the conditions are satisfied).

3. Values of Peclet and Damkohler numbers should be obtained from experiments.

4. Value of new porosity should be calculated.

3.2 Mobilization and retention of particles

3.2.1 Mobilization of particles

The two main factors, which govern the rate of mobilization of particles are:

1) rate of dissolution of calcium carbonate: calcium carbonate acts like a cement, which prevents particles from going into reservoir fluid and form a suspension. So, rate of mobilization of particles could be expressed as a fraction of rate of dissolution of calcium carbonate.

2) velocity of reservoir fluid (see 2.4.2).

3.2.2 Retention of particles

There are different mechanisms which govern retention of big and small particles.

3.2.2.1 Retention of small particles

There are a lot of mechanisms (see 2.4.3), which contribute in process of retention of particles. It is very difficult to include every single process in the model, therefore we will describe all of them in complex.

There are some models, which can be used for describing transport and retention of small particles:

1. System of equations [9]:

$$\begin{cases} \frac{\partial C}{\partial T} + \frac{\partial C}{\partial X} = -\frac{\partial S}{\partial T} \\ \frac{\partial S}{\partial T} = \Lambda(S)C \\ U = -\frac{k_0}{\mu(1+\beta\sigma)L}\frac{\partial p}{\partial X} \end{cases} \quad (3.12)$$

where X – dimensionless length,

$$X = \frac{x}{L}, \quad (3.13)$$

T – dimensionless time,

$$T = \frac{1}{L\varphi}\int_0^t U(t)dt, \quad (3.14)$$

C – dimensionless suspended particle concentration,

$$C = \frac{c}{c^0}, \quad (3.15)$$

S – dimensionless deposited particle concentration,

$$S = \frac{\sigma}{\varphi c^0}, \tag{3.16}$$

Λ – dimensionless filtration coefficient,

$$\Lambda = \lambda L, \tag{3.17}$$

L – core length,

U – velocity,

c^0 – injected suspended particle concentration,

σ – deposited particle concentration,

β – blocking parameter,

λ – filtration coefficient,

$$\frac{1}{\lambda} = \frac{\int_0^\infty xc(x,t)dx}{\int_0^\infty c(x,t)dx}. \tag{3.18}$$

The first two equations in system represent the kinematic of particle transport and capture; the third equation is a dynamical model that predicts pressure gradient increase due to permeability decline with particle deposition.

The solution of this system of equation is:

$$C(X,T) = e^{-\lambda X}, \tag{3.19}$$

$$S(X,T) = \lambda(T-X)e^{-\lambda X}. \tag{3.20}$$

2. Rate of deposition model [13]:

The total flux per pore per unit time is:

$$j_p = 2\pi DrC\left(\frac{U_R l^2}{Dr}\right)^{\frac{1}{3}}, \quad (3.21)$$

where D – diffusivity,

$$D = \frac{k_B \cdot T}{3\pi\eta d_p}, \quad (3.22)$$

k_B – Boltzmann's constant, $k_B = 1.38 \cdot 10^{-23}$ J/K,

η – viscosity,

d_p – diameter of particles,

r – pore radius,

C – concentration of particles in suspension,

U_R – fluid velocity in a pore with radius r,

l – pore length.

The rate of deposition per unit of time:

$$R_{dep} = 2\pi D^{\frac{2}{3}} l^{\frac{2}{3}} C \int (r^2 U_R)^{\frac{1}{3}} P_{pore} dr, \quad (3.23)$$

where P_{pore} – pore size distribution function.

Now we assume that pore length is equal to pore radius and fluid velocity is constant in all pores. Performing summation instead of integration:

$$R_{dep} = 2\pi D^{\frac{2}{3}} U_R^{\frac{1}{3}} C \Delta r \sum_{i=1}^{n} r_i^{\frac{4}{3}} P_{pore}. \quad (3.24)$$

For further calculations we will use the rate of deposition model.

3.2.2.2 Retention of big particles

The most probable mechanism for big particles to be retained is to stuck in the pore throats.

The “one-third one-seventh” criterion in filtration theory says [2] that particles smaller than one-seventh of the pore size flow in the filter without being captured, particles larger than one-third of the pore size are captured in the filter inlet and do not enter the filter, and the intermediate size particles perform deep bed filtration with non-zero probability to be captured.

3.3 Description of model

Main steps:

1. Modeling of distribution of pores
2. Modeling of distribution of particles
3. Calculation of average traveling distance for each particle size
4. Calculation of geometry of cylindrical model
5. Calculation of volume of calcium carbonate dissolved
6. Calculation of volume of big particles moved to next cell
7. Calculation of volume of small particles moved to next cell
8. Calculation of new porosities and permeabilities for each cell for each time step

Full script of program (written on MatLab) for this model with comments can be found in appendix A.

3.3.1 Modeling of pore and particle distribution

As long as we do not have actual data about pore and particle distribution we have to model it. We use normal distribution with the following parameters:

for pores:

- min value: 20 micrometers,
- max value: 320 micrometers,
- mean value: 170 micrometers,
- variance: 80 micrometers;

for particles:

- min value: 1 micrometers,
- max value: 1000 micrometers,
- mean value: 500 micrometers,
- variance: 200 micrometers;

Probability density function and cumulative distribution function of pore and particle distribution are shown on figures 3.1 and 3.2 respectively.

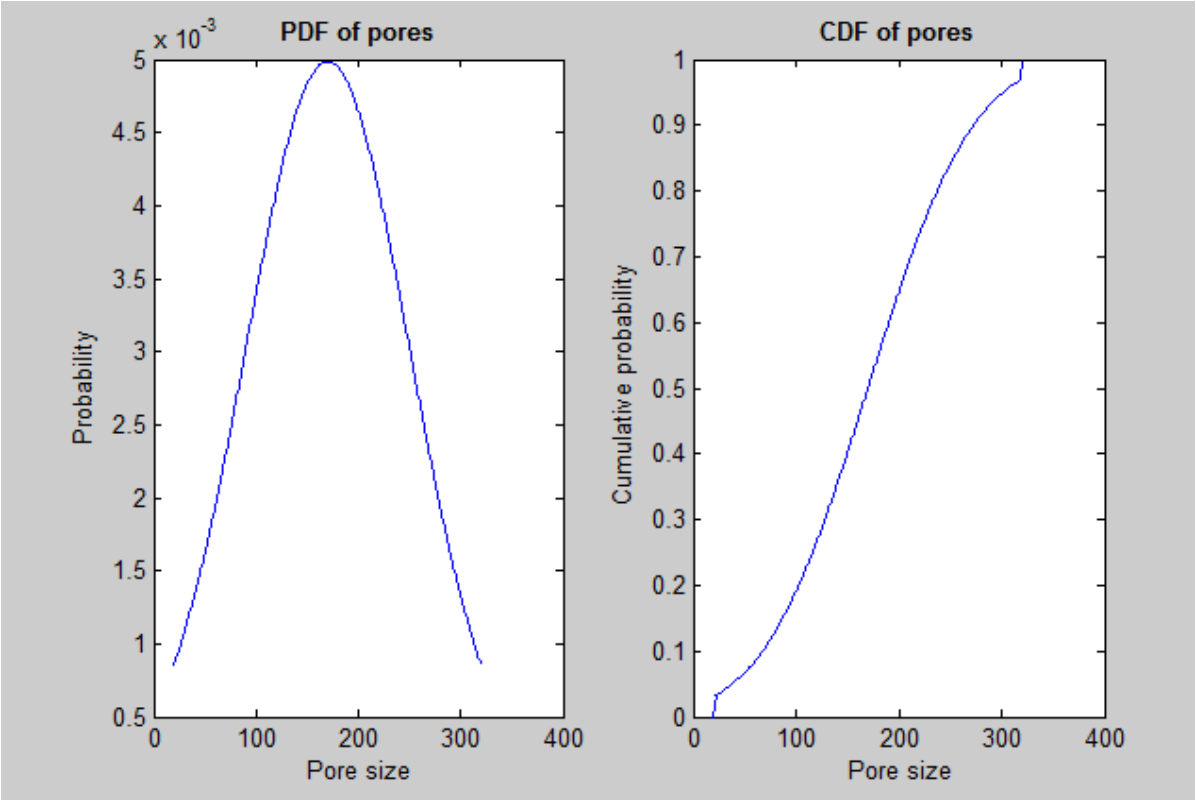

Figure 3.1 - Pore distribution

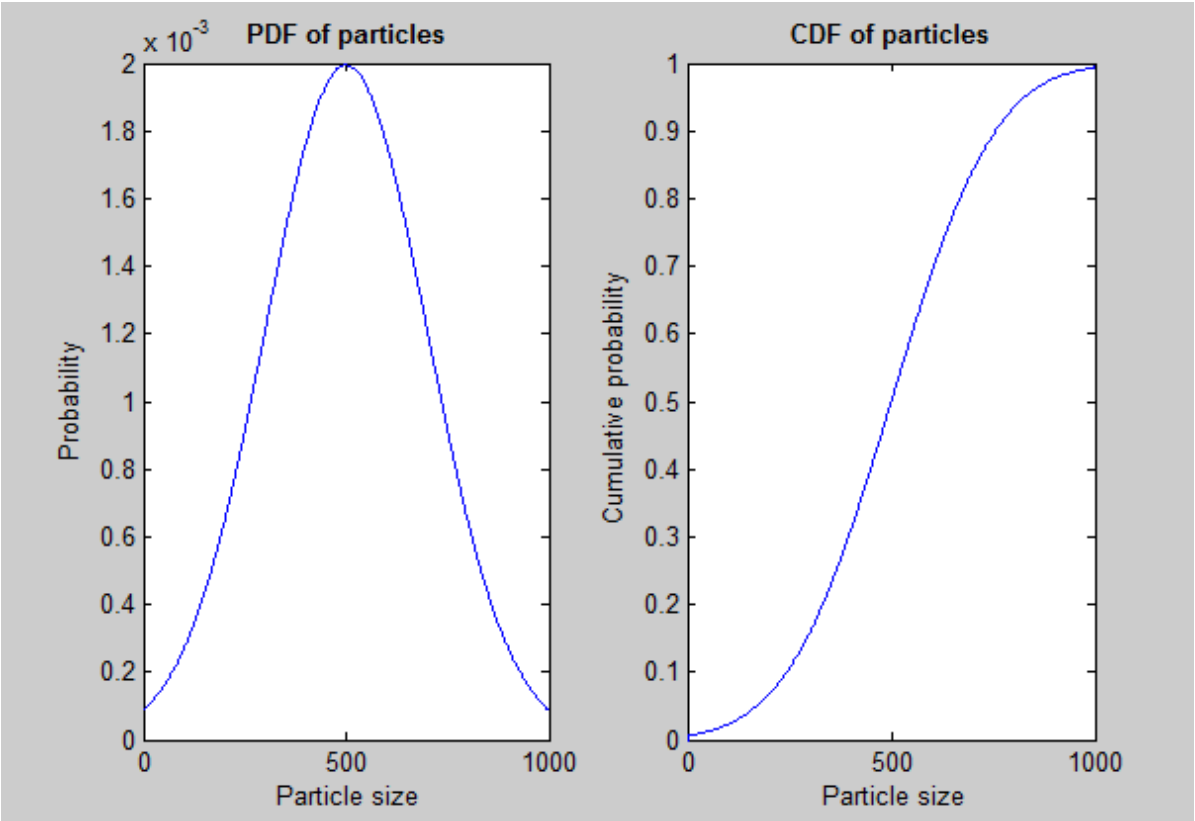

Figure 3.2 - Particle distribution

3.3.2 Big and small particles

We will call particles, which can move through rock with flow of CO_2, but could stuck in pore throat, the "big" particles. The particles, which can flow through any pore, we will call "small" particles. To determine the range of big particles we will use the "one-third one-seventh" criterion (see 3.2.2.2).

The maximum diameter of big particles:

$$d_{b\ max} = \frac{d_{pore\ max}}{3}, \tag{3.25}$$

where $d_{pore\ max}$ – diameter of the biggest pore.

The minimum diameter of big particles:

$$d_{b\ min} = \frac{d_{pore\ min}}{7}, \tag{3.26}$$

where $d_{pore\ min}$ – diameter of the smallest pore.

Movable particles include big and small particles. It is also comfortable for further calculation to calculate distributions of movable and big particles. We do it by assuming that CDF for $d_{b\ max}$ is equal to unity and then we adjust CDF and PDF for all other particle sizes. PDF and CDF for big particles is shown on figure 3.3.

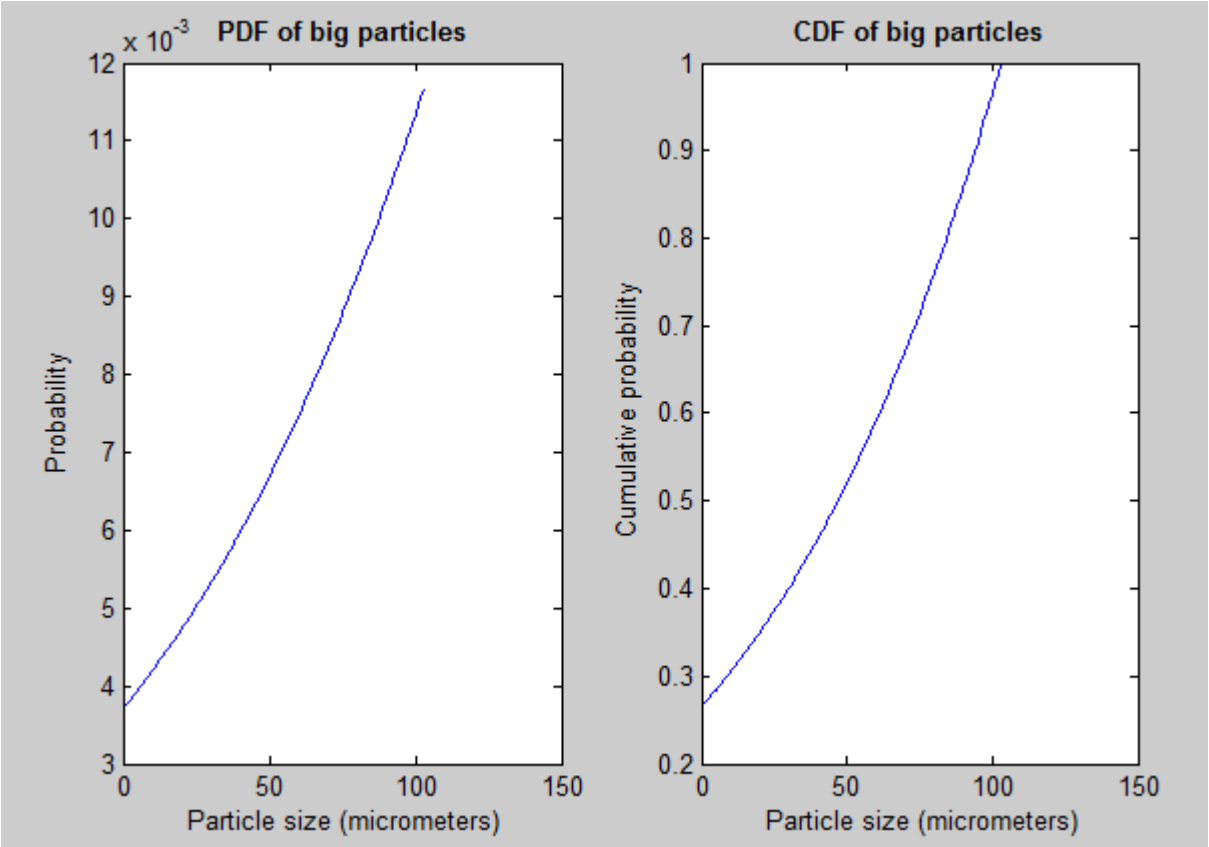

Figure 3.3 - Distribution of big particles

3.3.3 Calculation of average traveling distance for each particle size

Algorithm for each particle size:

1) randomly (according to pore distribution) choose size of first pore;

2) compare this pore size with size of particle;

   a) if particle size is larger than 1/3 of pore size, particle stuck in pore,

   b) if particle size is smaller than 1/7 of pore size, particle go through the pore throat,

   c) if particle size is in between it can either stuck or go through, we assume that probability of these outcomes is uniformly distributed and we use random number to find whether particle stuck or not;

3) if particle can flow through this pore we add its diameter (we assume that diameter and length of pore is equal) to traveling distance of particle (thus traveling distance is the sum of pore diameters which particle has passed) and go to next pore;

4) if particle stuck in pore we go to next simulation case, in our program we use 1000 simulations for each particle size;

5) after all 1000 simulations for this particle size are completed, average traveling distance is calculated.

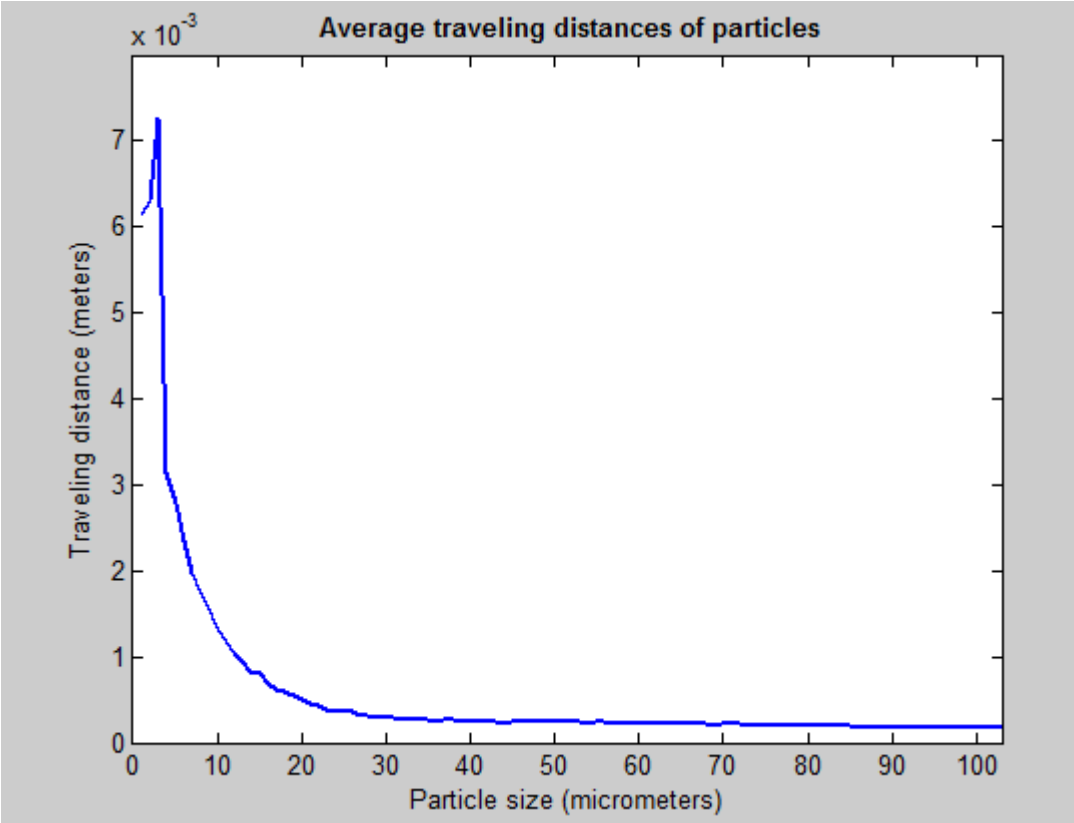

Figure 3.4 - Average traveling distances of particles

Figure 3.4 shows the average traveling distances for all particle sizes.

3.3.4 Geometry of cylindrical model

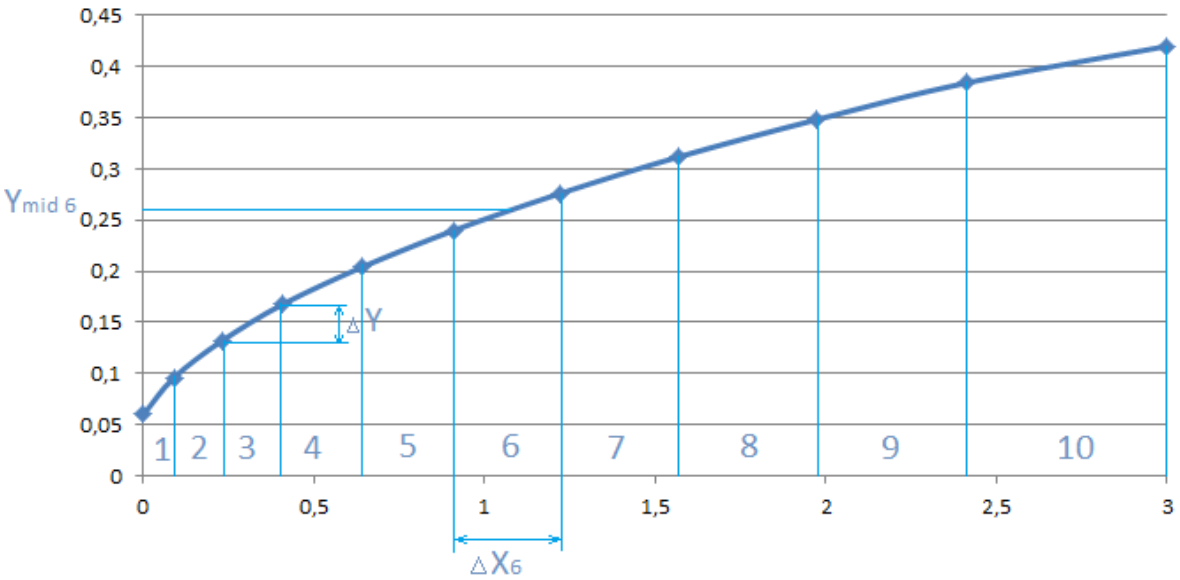

Figure 3.5 - Cross section of upper half part of cylindrical model

Actually our cylindrical model is not really cylindrical but looks more like parabolic. Exact shape of it will be explained later but it could be found according to the following formula:

$$y = 0.226\sqrt{\frac{w \cdot x}{r_w}}, \tag{3.27}$$

where w – mass rate of CO_2;

r_w – inlet radius.

Figure 3.5 demonstrates the cross section of upper part of model. Model is divided on 10 cells so that ΔY is constant for all cells. Opposite ΔX is unique for each cell. Y_{mid} could be found as an arithmetic mean between ordinates of borders of cell.

We assume that each cell is a cylinder with radius Y_{mid} and high ΔX. So the volume of each cell could be found according to formula:

$$V_{cell} = \pi \cdot Y_{mid}^2 \cdot \Delta X. \tag{3.28}$$

3.3.5 Velocity of fluid

Interstitial velocity of flow in a cell:

$$U = \frac{Q}{A}\varphi, \tag{3.29}$$

where φ – porosity;

Q – volumetric flow:

$$Q = \frac{w}{\rho}, \tag{3.30}$$

ρ – density of liquid,

A – cross section area:

$$A = \pi Y_{mid}^2, \tag{3.31}$$

so

$$U = \frac{w\varphi}{\pi\rho Y_{mid}^2}. \tag{3.32}$$

As long as cross section areas of cells in our model are not equal, the velocities of fluid are not equal either (but we assume that velocity is equal within one cell). Obviously velocity in the first ($U_{cell\ 1}$) cell (where the radius is smallest) is highest. To show the velocity dependence on different processes (dissolution of calcium carbonate, mobilization of particles) we implement the velocity coefficient, which is:

$$K_{veloc} = \frac{U_{cell\ i}}{U_{cell\ 1}}, \tag{3.33}$$

where $U_{cell\ I}$ – velocity in current cell.

3.3.6 Calculation of volume of calcium carbonate dissolved

Calculation is mainly based on procedure, described in 3.1.5. The main factors, which influence the rate of dissolution are velocity of flow and temperature.

As long as we do not have any experimental data regarding to velocity dependence, we assume that decreasing of velocity affects reaction rate coefficient for forward reaction proportional to velocity coefficient and reaction rate coefficient for backward reaction revers proportional to velocity coefficient:

$$k_{1\,v} = k_1 \cdot K_{veloc}, \tag{3.34}$$

$$k_{2\,v} = \frac{k_2}{K_{veloc}}. \tag{3.35}$$

Then we introduce the temperature dependence by formula 3.5 and calculate reaction rate with formula 3.10. Rate of reaction can be a negative value, it means that rate of forward reaction is less than rate of backward reaction, thus calcium carbonate precipitates from solution.

Finally, the volume is calculated by the formula:

$$V_{CaCO_3} = \frac{r \cdot M \cdot V_{rock} \cdot \varphi \cdot t_{st}}{\rho}, \tag{3.36}$$

where t_{st} – time step in calculations.

3.3.7 Calculation of volume of particles moved to next cell

3.3.7.1 Volume of mobilized particles

It depends on:

1. volume of calcium carbonate dissolved;
2. velocity of flow.

Calcium carbonate acts as cement which keeps particles on the rock surface. As calcium carbonate is dissolving, particles can easily be mobilized. So, volume of particles mobilized is proportional to volume of calcium carbonate dissolved. The proportionality coefficient is K_{part}. It should be determined experimentally.

Velocity plays a significant role in mobilization of particles. The higher the velocity the more likely particles are mobilized.

Thus volume of mobilized particles is:

$$V_{part} = V_{CaCO_3} \cdot K_{part} \cdot K_{veloc}. \quad (3.37)$$

3.3.7.2 Calculation of volume of big particles which moves to next cell

Changing of porosity in cell is caused by matter moving to next cell. Not all the mobilized particles moves to next cell at certain period of time (time step). Only particles, which are within average traveling distance from border of cell, can move to next cell. Thus total volume of big particles is:

$$V_{bp\ mov} = \sum_{i=d_{b\ min}}^{d_{b\ max}} \frac{V_{bp\ mob\ i} \cdot L_{av\ i}}{\Delta X}, \quad (3.38)$$

where $V_{bp\ mob\ i}$ – cumulative volume of mobilized particles of diameter i,

$$V_{bp\ mob\ i} = P_{bp\ i} \cdot V_{part}, \quad (3.39)$$

P_{bp} – probability density function of big particles,

$L_{av\ i}$ – average traveling distance of particles of diameter i.

3.3.7.3 Calculation of volume of small particles which moves to next cell

Volume of mobilized small particles is the volume of mobilized particles with the deduction of volume of mobilized big particles. If it is not the first cell, we also add the volume of small particles, which came from previous cell.

For calculation of volume of deposited particles we use equation 3.23 (multiplying rate on length of time step for to obtain volume).

Volume of small particles, which move to next cell, is volume of mobilized small particles with the deduction of volume of deposited small particles.

3.3.8 Calculation of new porosities

When matter, which previously was a part of rock, moves to other cells, volume of rock decreases and consequently volume of porous space increases, therefore porosity will increase. In the other hand, if it is not the first cell, matter can come from previous cells and if this coming amount larger than amount of matter moving to next cell porosity will decrease.

New porosity could be found as:

$$\varphi_{new} = \frac{V_{cell} \cdot \varphi + V_{CaCO_3} + V_{bp\ mov} + V_{sp\ mov} - V_{bp\ mov\ prev} - V_{sp\ mov\ prev}}{V_{cell}}, \quad (3.40)$$

where φ – previous porosity,

V_{cell} – volume of cell,

V_{CaCO3} – volume of dissolved (or precipitated – with negative sign) calcium carbonate,

$V_{bp\ mov}$, $V_{sp\ mov}$ – volume of big and small particles, moving to next cell,

$V_{bp\ mov\ prev}$, $V_{sp\ mov\ prev}$ - volume of big and small particles, coming from previous cell.

New porosities should be calculated for each cell and for each time step.

Figure 3.6 shows changing in porosity in our simulation case. As we can see at last time step porosity becomes higher in cells from first to third, at fourth cell porosity remains the same and after fifth cell porosity decreasing.

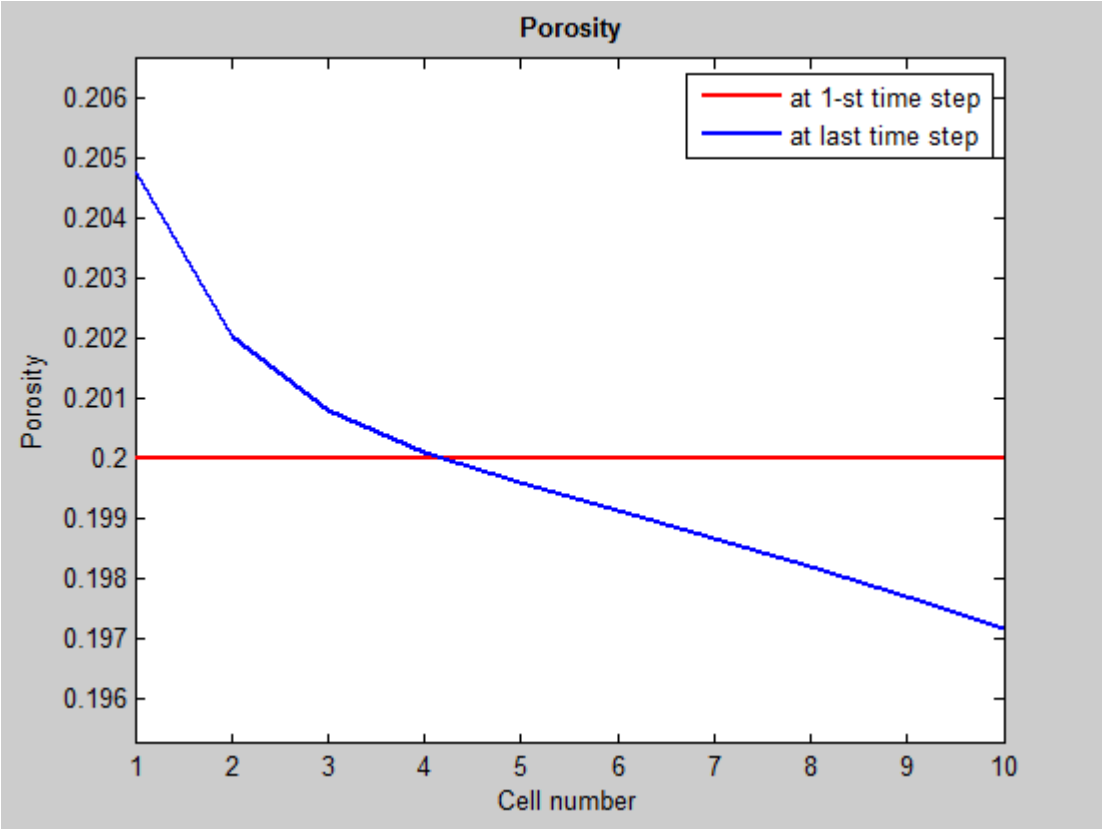

Figure 3.6 - Changes in porosity

3.3.9 Calculation of new permeabities

For calculation of permeability we will use Kozeny-Carman model [10]:

$$k_{new} = k\left(\frac{\varphi_{new}}{\varphi}\right)^{c}\left(\frac{1-\varphi}{1-\varphi_{new}}\right)^{2}, \tag{3.41}$$

where c – exponent, depends on rock type.

Figure 3.7 shows changing of permeability in our simulation case. As we can see trend of changes repeats changes in porosity.

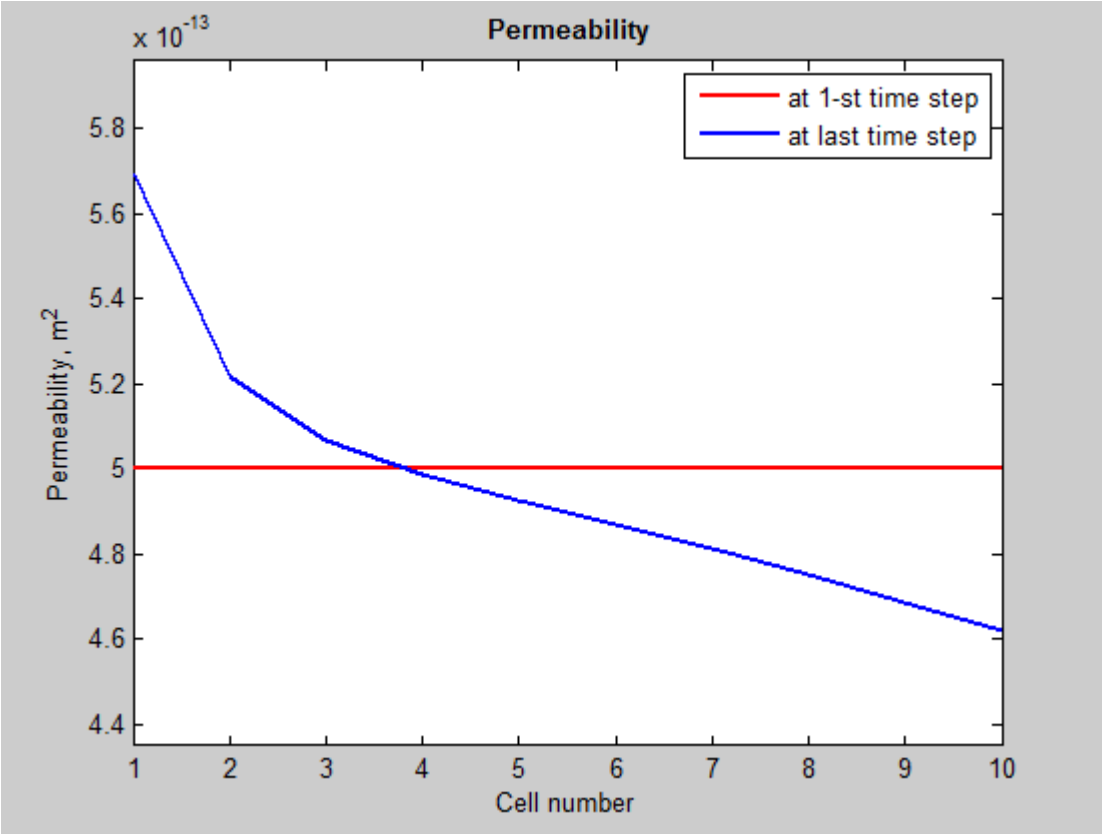

Figure 3.7 - Changes in permeability

4 SIMULATION

This chapter deals with mechanical models and computer simulation of injection of carbon dioxide into these models. The changing of permeability distribution with time, obtained from the program, described in previous chapter, was used during simulation.

4.1 Mechanical models

There are two mechanical models considered – cake-slice model and cylindrical-cone model. One of the goals of computer simulation is to show that they behave similarly and the one can be replaced by the other.

4.1.1 Cake-slice model

Model resembles the radial flow behavior in cylindrical reservoir geometry. The main parameters of model (figure 4.1):

r_w – the well radius;

r_e – the boundary (outer) radius;

h – the cake-slice height;

α – slice angle.

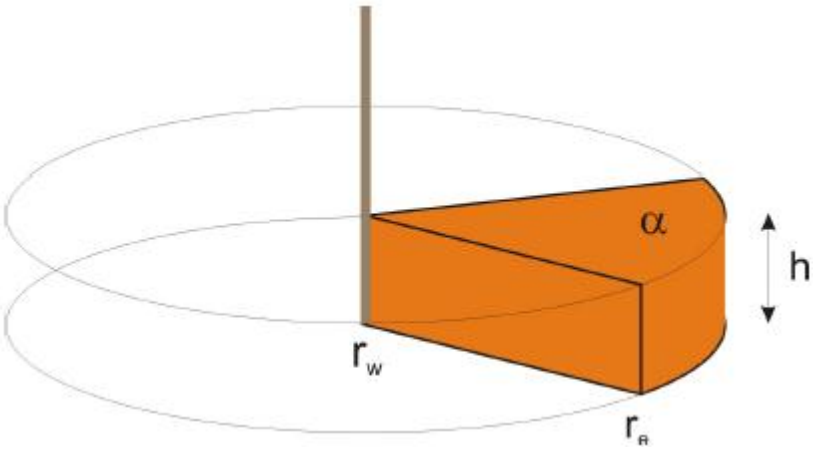

Figure 4.1 - Cake-slice model

Parameters of model should be defined in the way, that experiment is properly scaled and express reservoir properties correctly. For this purpose an injection pressure gradient is used [17]:

$$IPG = max\left\{\left|\frac{dp}{dr}\right|\right\} = \frac{w(\mu/\rho)}{2\pi hk}\frac{1}{r_w}, \quad (4.1)$$

where w – the mass flow,

μ – viscosity,

ρ – density,

k – permeability.

An injection pressure gradient for our model is:

$$IPG_{model} = \frac{w(\mu/\rho)}{(2\pi/360)\alpha hk}\frac{1}{r_w}. \quad (4.2)$$

Using formula 4.2 and data from table 4.1 we can define the main parameters of cake model (figure 4.2).

Table 4.1. Typical reservoir and fluid data

Property	**Value**
Permeability, k	500 – 800 mD
Well radius, r_w	0.05 m
Mass flow, w	0.007 – 0.07 kg/s
Viscosity/density, $(\mu/\rho)_{CO2}$	$8 \cdot 10^{-8}$ Pa·s/(kg/m^3)
IPG	10^6 Pa/m

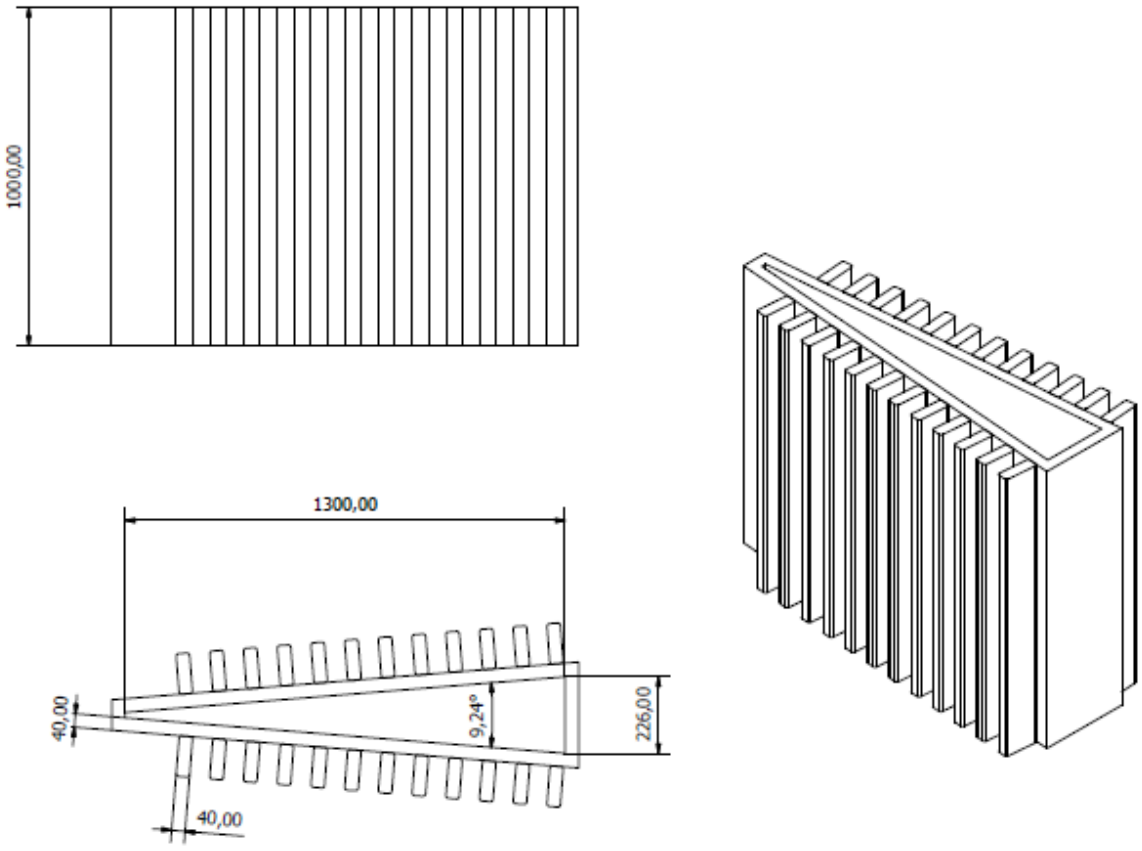

Figure 4.2 - Setup for cake-slice model

After stress analysis it was found, that the cake-slice model has the unfavorable combination of high pressures and large straight surface areas [17]. Straight surfaces will bend under the influence of high pressures. Figure 4.3 shows the stress distribution in model.

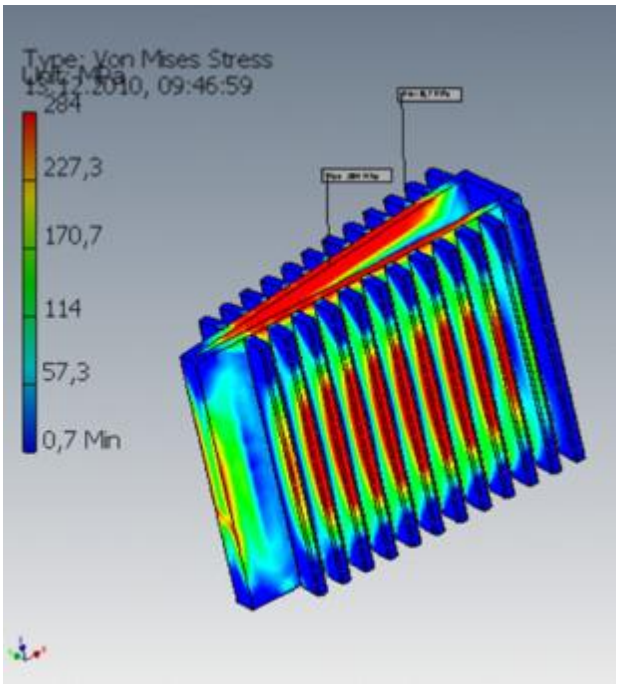

Figure 4.3 - The stress distribution in cake-slice model

4.1.2 Cylindrical-cone model

Because too high stresses in cake-slice model alternative solutions have to be found. The main parameter, which has to be preserve in new model, is the increasing flow area. Cylindrical-cone model was chosen.

Cross sectional area of cake-slice model is:

$$A_{c-s} = \theta r h, \tag{4.3}$$

where θ – the space angle, measured in radians,

$$\theta = \frac{2\pi}{360}\alpha. \tag{4.4}$$

Cross sectional area of cylindrical-cone model is:

$$A_{c-c} = \pi R^2, \tag{4.5}$$

where R – variable radius of cylindrical tube.

For to satisfy the condition $A_{c\text{-}s}$ has to be equal $A_{c\text{-}c}$, thus:

$$R = \sqrt{\frac{\theta r h}{\pi}}. \tag{4.6}$$

Combining this equation with equation 4.2:

$$R = \sqrt{w \frac{1}{\pi} \frac{(\mu/\rho)}{k \cdot IPG} \frac{r}{r_w}}. \tag{4.7}$$

Using data from table 4.1:

$$R = 0.226 \sqrt{w \frac{r}{r_w}}. \tag{4.8}$$

This cylindrical-cone model has actually a shape of function $y = \sqrt{x}$ (parabolic-like shape), because $R \sim \sqrt{r}$ (figure 4.4).

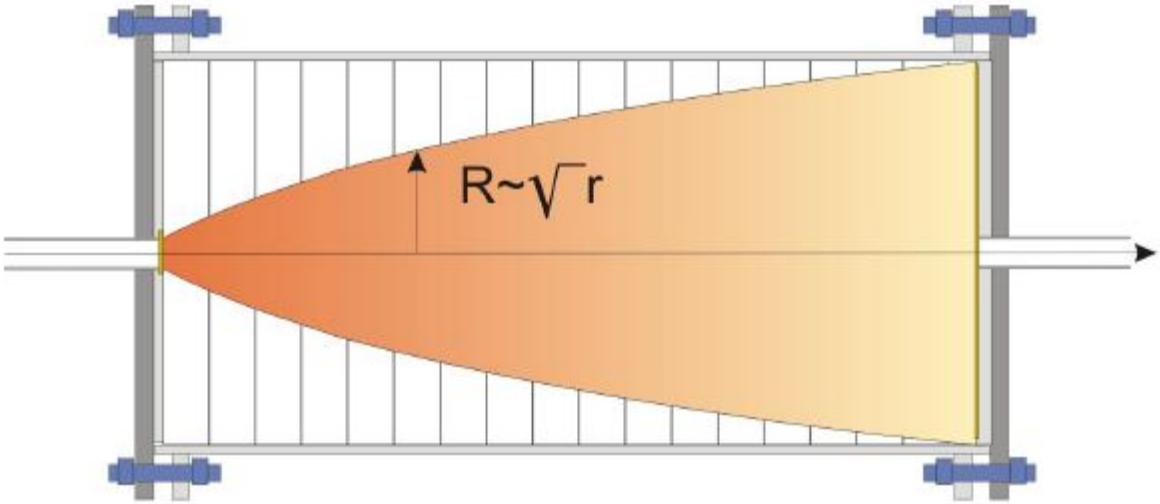

Figure 4.4 - Cylindrical-cone model

For simulation we will use both slice-cake and cylindrical-cone model.

4.2 Simulation in CMG Stars

The main sets of parameters, which has to be specified for model:

1. Grid parameters;

2. Fluid and rock parameters;

3. Well specification;

4. Time steps for report and parameters changing in time.

Data-files for simulation with initial parameters could be found in appendixes B and C.

4.2.1 Grid

4.2.1.1 Grid specification for slice-cake model

It is natural to use radial type of grid for simulation slice-cake model. Parameters of grid and properties of cells could be found in table 4.2.

Figure 4.5 shows right half of cross section of model and figure 4.6 shows 3D view of model.

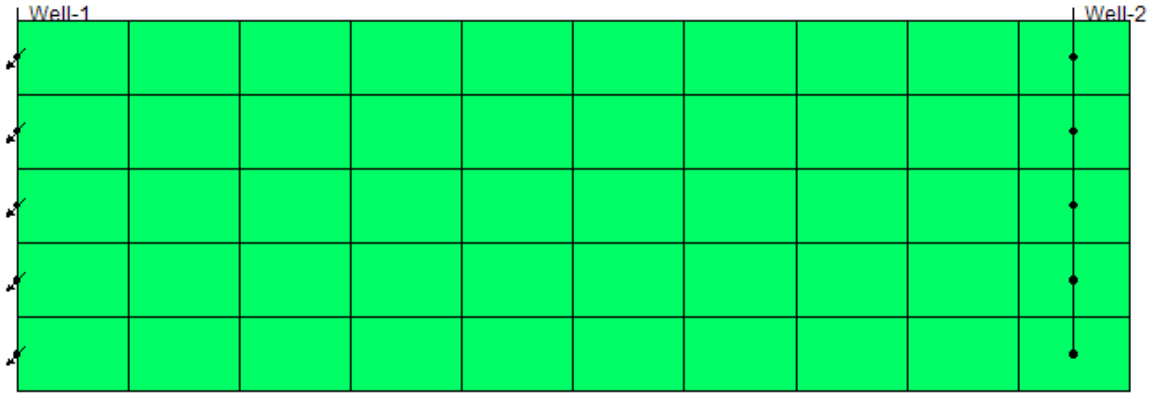

Figure 4.5 - Cross section of the cake-slice model (right half)

Table 4.2. Grid parameters and properties of cells

Parameter	**Value**
Number of cells in R-direction	10
Number of cells in θ-direction	1
Number of cells in Z-direction	5
Length of cells in R-direction, m	0.3
Angle of model in θ-direction, degrees	9.24
Height of cells in Z-direction, m	0.2
Depth of the top layer of the grid, m	1000
Porosity	0.2
Permeability in R-direction, mD	500
Permeability in θ-direction, mD	500
Permeability in Z-direction, mD	500

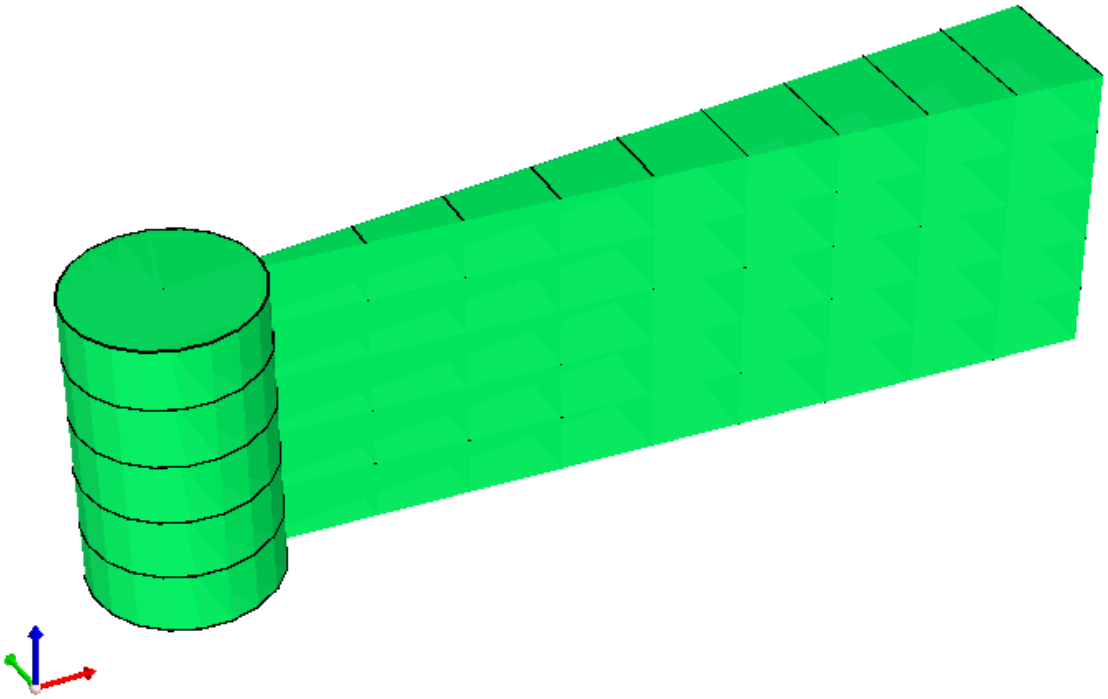

Figure 4.6 - 3D view of cake-slice model

4.2.1.2 Grid specification for cylinder-cone model

For this model we will also use radial type of grid, but with volume modification. First we will construct usual grid and then cut part of it for to achieve parabolic shape as close as possible.

Parameters of grid and properties of cells could be found in table 4.3.

Figure 4.7 shows top half of cross section of model and figure 4.8 shows 3D view of model.

Table 4.3. Grid parameters and properties of cells

Parameter	**Value**
Number of cells in R-direction	12
Number of cells in θ-direction	4
Number of cells in Z-direction	10
Length of cells in R-direction, m	0.0365
Angle of model in θ-direction, degrees	90
Height of cells in Z-direction, m	0.09, 0.14, 0.18, 0.23, 0.27, 0.31, 0.35, 0.4, 0.44, 0.59
Depth of the top layer of the grid, m	1000
Porosity	0.2
Permeability in R-direction, mD	500
Permeability in θ-direction, mD	500
Permeability in Z-direction, mD	500

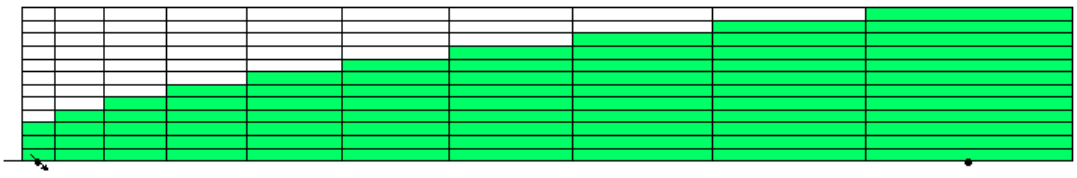

Figure 4.7 - Cross section of the cake-slice model (top half)

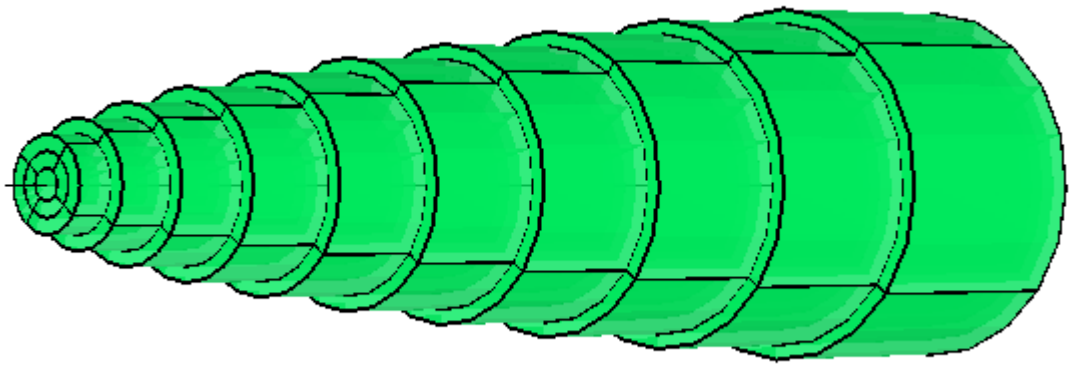

Figure 4.8 - 3D view of cake-slice model

Volume modification:

1) cells, which are inside the model, remain with the same volume;

2) cells, which are on the border of model, are cut by half, forming a triangle in cross section;

3) cells, which are out of the model, get 0 as a value of volume.

Figure 4.9 shows the volume of cells in model. As we can see on the borders volumes of cells as twice as less then volume of neighbor cell, which is inside model.

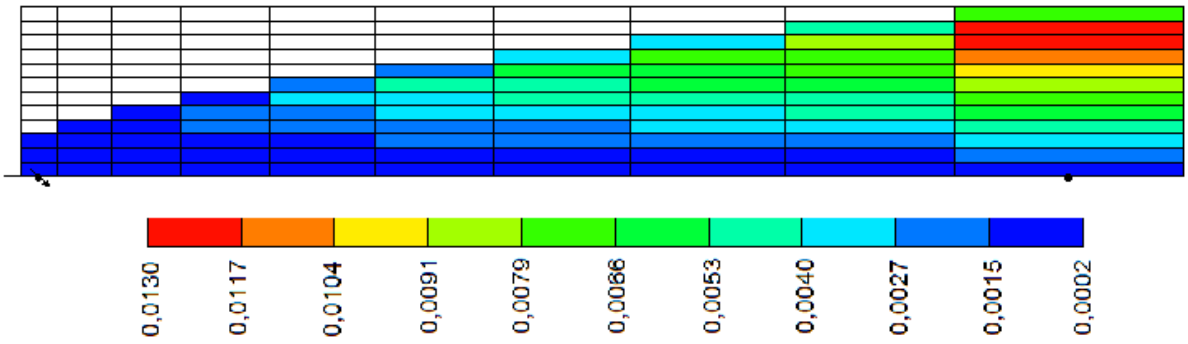

Figure 4.9 - Volume of cells in the model

4.2.2 Rock and fluid properties

The main fluid properties are shown in table 4.4.

Table 4.4. The main fluid properties

Property	**Value for water***	**Value for CO_2***
Molecular weight, kg/gmol	0.018	0.048
Critical pressure, kPa	0	4595.71
Critical temperature, C	374.15	31.05
Density, kg/m^3	1050	2
Viscosity (20 C), cP	1	0.1177
Compressibility, 1/kPa	$5 \cdot 10^{-6}$	$9.73 \cdot 10^{-7}$

* Values are taken from [5]

Figure 4.10 shows relative permeabilities for water and carbon dioxide.

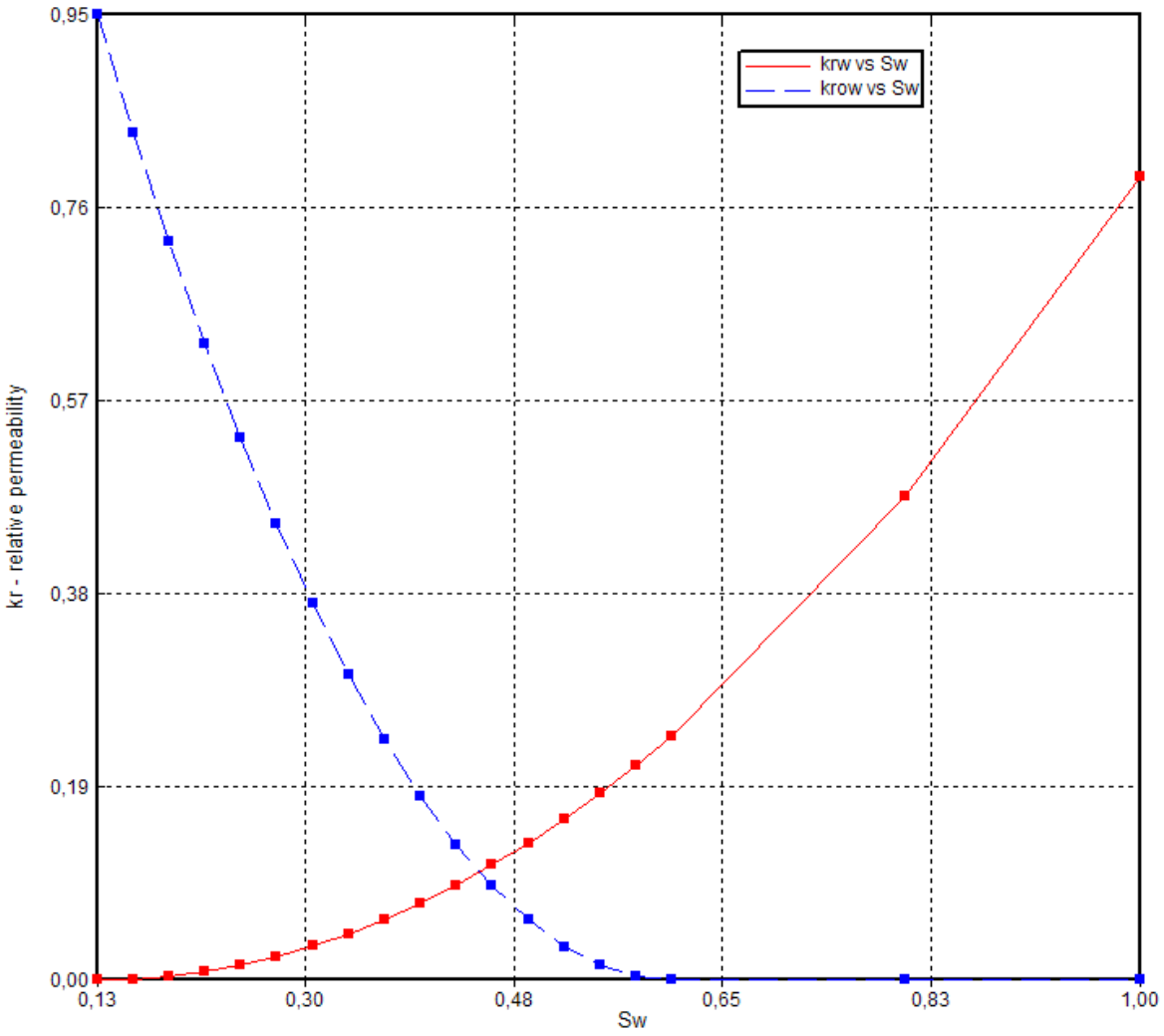

Figure 4.10 - Relative permeabilities for water and CO_2

Figure 4.11 shows temperature dependence for water and carbon dioxide viscosities.

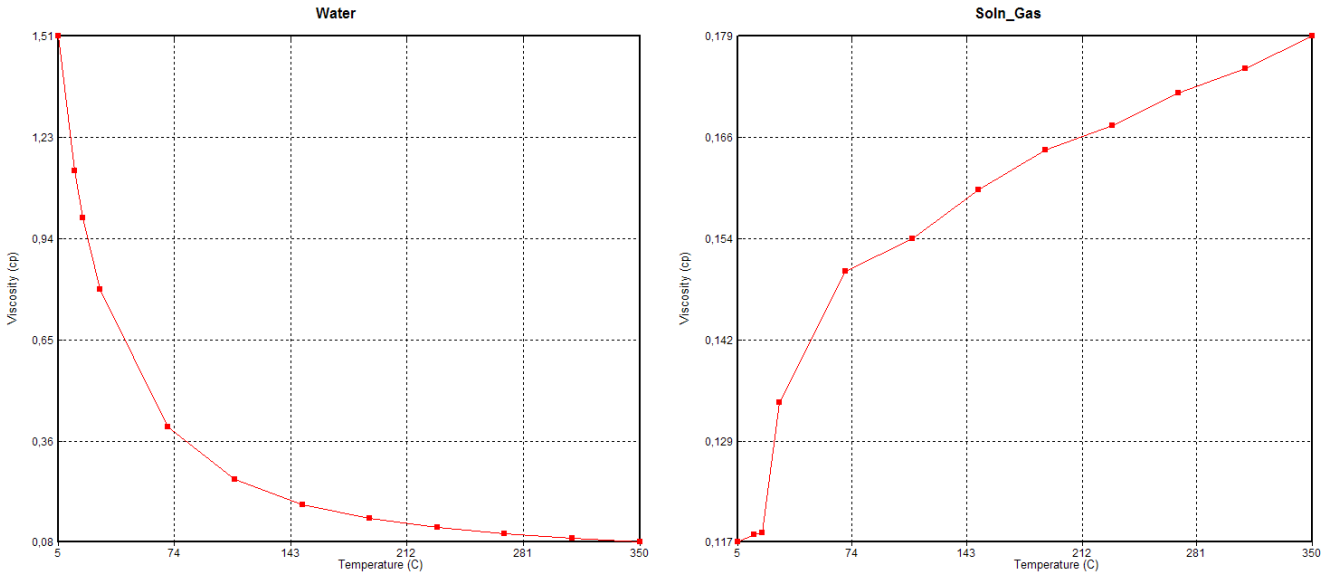

Figure 4.11 - Viscosity vs. Temperature for water and CO_2

4.2.3 Well specification

There are two wells present in both cases – injector and producer.

The main property of injector is stock tank cubic meters of gas (STG) injected. If we have mass rate of 0.007 kg/s, STG will be 302.4 m^3/s.

The main property of producer is bottom hole pressure (BHP), which in our case is 7000 kPa.

These constraints (STG and BHP) and properties of rock and fluid regulate pressure distribution in reservoir.

4.2.4 Parameters changing in time

During the injection of carbon dioxide because of calcium carbonate dissolution and precipitation and particles migration permeability changes in reservoir.

In CMG Stars there is only one way to change permeability during simulation – to change mobility with mobility multipliers. As long as properties of liquid remain unchanged, it is possible to change permeability by changing mobility.

5 RESULTS

As a result parameter we will use pressure in reservoir (model). We will use pressure data, taken from the middle of models, for all 10 cells in different periods of time.

5.1 Comparison of results for slice-cake and cylindrical-cone models

There is a slight difference in numbers for pressure distribution for two models, but this difference is negligible. Figure 5.1 shows relative pressure difference (in percent) between two models.

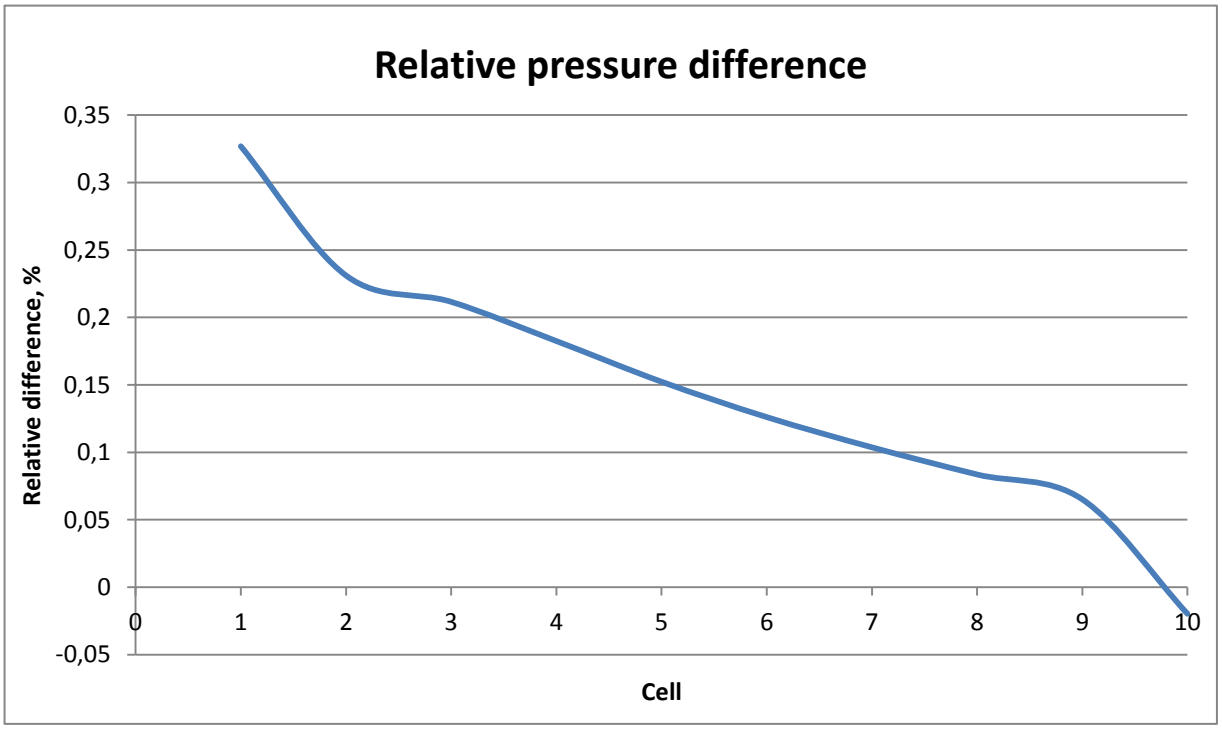

Figure 5.1 - Relative pressure difference between slice-cake and cylindrical-cone model

As we can see relative difference does not exceed 0.33%, which is pretty much acceptable. It means that we can conceder these two models as equal.

5.2 Comparison of results for cases with changing and constant permeability

Figures 5.2 and 5.3 show us a pressure difference between cases with changing and constant permeability for cylindrical-cone and slice-cake models. We can see that changes have a similar trend. For explanation of this behavior of curves we should remember the trend of changing of permeability (figure 5.4).

We can see that near the cell number 4 permeability remains almost constant. Permeability increases sharply towards the injection well (first cell) and decreases smoothly towards the production well (last cell).

Pressure is constant at the production well. Towards the injection well pressure difference increases smoothly because of decreased permeability at this region. Near the cell number four we can observe a peak after which pressure difference decreases more or less fast.

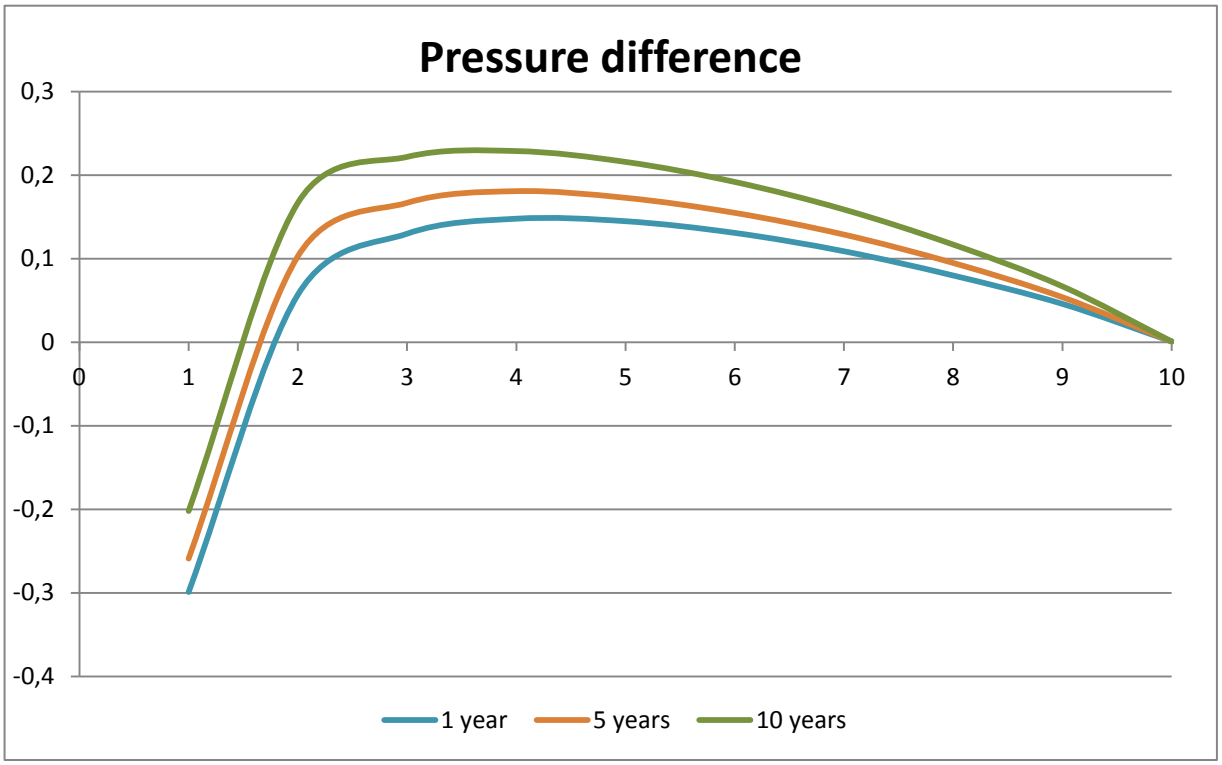

Figure 5.2 - Pressure difference between cases with changing and constant permeability for cylindrical-cone model

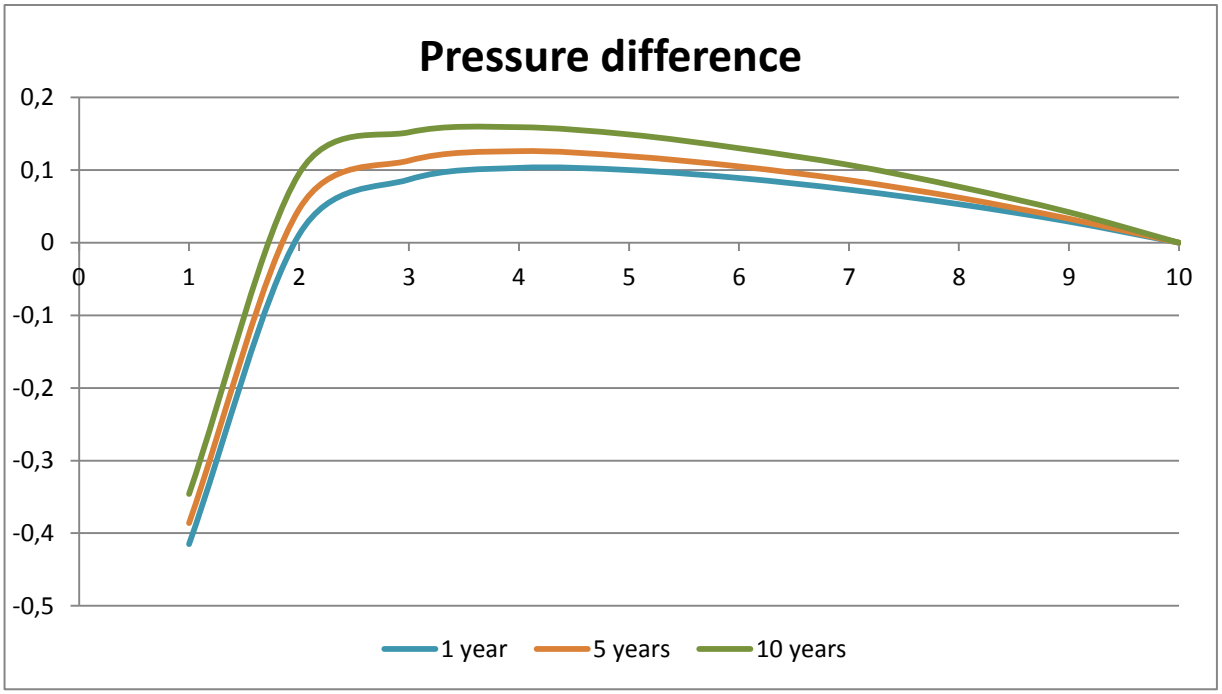

Figure 5.3 - Pressure difference between cases with changing and constant permeability for slice-cake model

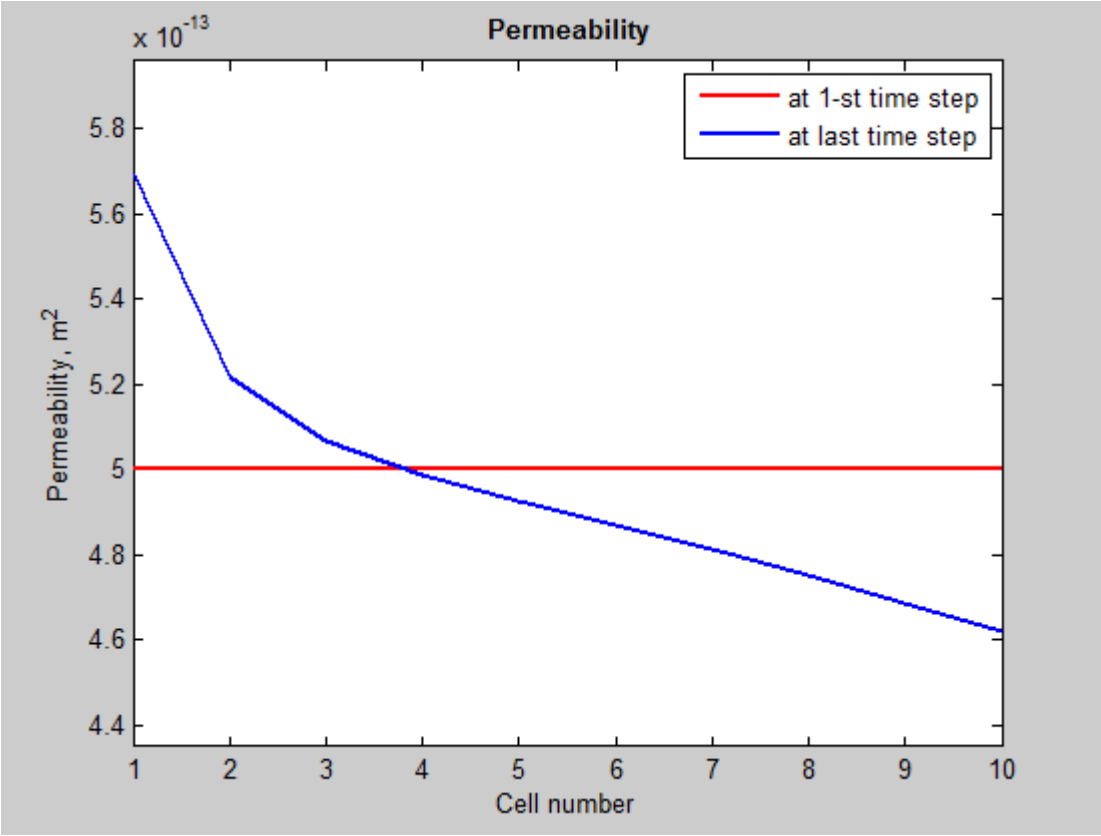

Figure 5.4 - Changes in permeability

6 CONCLUSIONS AND RECOMMENDATIONS FOR FUTURE WORK

The processes of migration of particles and dissolution and precipitation of carbonates during CO_2 injection and their influence on injectivity (pressure distribution in reservoir) have been investigated in this thesis.

Mathematical model of these processes was developed and implemented in MatLab-program. As a result of work of program we get a new permeability distribution in reservoir. We can observe that permeability increases dramatically near injector, but decreases further away in reservoir.

These data about new permeabilities are implemented in computer simulation (in CMG Stars). The main results of simulation:

1) pressure distribution is almost the same for slice-cake and cylindrical-cone models, which means that we can use either of them for description of physical processes in reservoir;

2) trend of changing of pressure distribution is consistent with trend of changing of permeability distribution in reservoir.

Thus we can conclude that injection of CO_2 had an influence on permeability and pressure distribution in reservoirs and consequently on injectivity.

Because we did not have possibility to conduct some necessary experiments, during development of mathematical model and simulation we had to use some assumptions. Therefore our recommendation for future work is to conduct these experiments and implement the results (which should be fairly easy to do). In particular future investigations could be:

1) to conduct experiments for to obtain:

   - rate constants for forward and backward reactions,
   - activation energy,

- velocity dependence;

2) to find experimentally the fraction of mobilizes particles (caused by calcium carbonate dissolution);

3) deeper research about retention of small particles.

7 REFERENCES

1. Baklid A., Korbøl R. Sleipner vest CO_2 disposal, CO_2 injection into a shallow underground aquifer. Paper SPE 36600 was presented in Denver, USA, 1996.

2. Bedrikovetsky P.G., Monteiro S.P., Neto A.M.M., Riente A.F. Fractional flow theory for suspension flow in petroleum reservoirs. Paper SPE 121822 was presented in Cartagena, Colombia, 2009.

3. Cailly B. Geological storage of CO_2: a state-of-the-art of ingection processes and technologies. Oil and gas science and technology, 2005.

4. Chauveteau G., Nabzar L., Coste J-P. Physics and modeling of permeability damage included by particle deposition. Paper SPE 39463 was presented in Lafayette, USA, 1998.

5. Computer modeling group (CMG): CMG STARS user's guide. Calgary, Canada, 2009.

6. Egermann P., Bazin B., Vizika O. An experimental investigation of reaction-transport phenomena during CO_2 injection. Paper SPE 93674 was presented in Bahrain, 2005.

7. Gabriel G.A., Inamdar G.R. An experimental investigation of fines migration in porous media. Paper SPE 12168 was presented in San Francisco, USA, 1983.

8. Gruesbeck C., Collins R.E. Entrainment and deposition of fine particles in porous media. Paper SPE 8430 was presented in Las Vegas, 1982.

9. Guedes R.G., Al-Abduwani F.A., Bedrikovetsky P.G., Currie P.K. Injectivity decline under multiple particle capture mechanisms. Paper SPE 98623 was presented in Lafayette, USA, 2006.

10. Izgec O., Demiral B., Bertin H., Akin S. Experimental and numerical modeling of direct injection of CO_2 into carbonate formations. Paper SPE 100809 was presented in San Antonio, USA, 2006.

11. Nabzar L., Chauveteau G., Roque. A new model for formation damage by particle retention. Paper SPE 31119 was presented in Lafayette, USA, 1996.

12. Roque C., Chauveteau G., Renard M., Thibault G., Bouteca M. Mechanism of formation damage by retention of particles suspended in injection water. Paper SPE 30110 was presented in Hauge, Netherlands, 1995.

13. Sharma M.M., Yortsos Y.C., Handy L.L. Release and deposition of clays in sandstone. Paper SPE 13562 was presented in Phoenix, USA, 1985.

14. Sharma M.M., Yortsos Y.C. Permeability impairment due to fines migration in sandstones. Paper SPE 14819 was presented in Lafayette, USA, 1986.

15. Sifuentes W., Blunt M.J., Giddins M.A. Modeling CO_2 storage in aquifers: assessing the key contributors to uncertainty. Paper SPE 123582 was presented in Aberdeen, UK, 2009.

16. Svec R.K., Grigg R.B. Physical effect of WAG fluids on carbonate core plugs. Paper SPE 71496 was presented in New Orleans, USA, 2001.

17. Ursin J. R. Modeling of well – reservoir interfacial couplings. Stavanger, Norway, 2011.

18. Carbonate dioxide and carbonic acid. Available on the site of Utah state university:
http://www.chem.usu.edu/~sbialkow/Classes/3650/Carbonate/Carbonic%20Acid.html

APPENDIX A. Script of MatLab program

```
%%%%%%%%%%%%%%%%%%%%%%%%%%%%%%%%%%%%%%%%%%%%%%%%%%%%%%%%%%%%%%%%%%%%%%%%%%%%%%%
%%%  This program calculates changing of permeability caused by       %%%
%%%  migration of particles and dissolution of calcium carbonate      %%%
%%%  during carbon dioxide injection                                  %%%
%%%%%%%%%%%%%%%%%%%%%%%%%%%%%%%%%%%%%%%%%%%%%%%%%%%%%%%%%%%%%%%%%%%%%%%%%%%%%%%

%%% Preparing of memory space
clc
clear

%%% Preparing of initial data
w=0.007;              % kg/s - mass rate of CO2
rw=0.06;              % m - inlet radius of cylindrical model
R=8.31;               % J/mol*K - gas constant
T=350;                % K - reservoir temperature
k01=3*10^(-9);        % reaction rate coefficient for forward reaction
k02=10^(-10);         % reaction rate coefficient for backward reaction
Ea1=-25000;           % J/mol - activation energy of forward reaction
Ea2=-25000;           % J/mol - activation energy of backward reaction
MCaCO3=0.1;           % kg/mol - molar mass of CaCO3
roCaCO3=2710;         % kg/m3 - density of CaCO3
fi=0.2;               % porosity
Kpart=2;              % fraction of particles mobilized
minpod=20;            % mkm - min pore diameter
maxpod=320;           % mkm - max pore diameter
minpad=1;             % mkm - min particle diameter
maxpad=1000;          % mkm - max particle diameter
visc_co2=2*10^(-6);   % Pa*s - viscosity of CO2
ro_co2=500;           % kg/m3 - density of CO2
t_step=3600*24*36;    % s - time step
tot_time=3600*24*360; % s - time of simulation
k=500*10^(-15);       % m2 - permeability

%%%%%%%%%%%%%%%%%%%%%%%%%%%%%%%%%%%%%%%%%%%%%%%%%%%%%%%%%%%%%%%%%%%%%%%%%%%%%%%

%%% Modeling of distrebution of pores
pore_diam=[minpod:1:maxpod];           % We assume that pores are
pore_N=length(pore_diam);              % distributed normally with
pore_pdf=normpdf(pore_diam,170,80);    % mu=170 and sigma=80
pore_cdf=normcdf(pore_diam,170,80);
pore_cdf(1)=0;
pore_cdf(pore_N)=1;

figure(1)
subplot(1,2,1)
plot(pore_diam,pore_pdf)
title('\bf PDF of pores ')
xlabel(' Pore size (micrometers)')
ylabel(' Probability')
subplot(1,2,2)
plot(pore_diam,pore_cdf)
title('\bf CDF of pores ')
xlabel(' Pore size (micrometers)')
```

```
ylabel(' Cumulative probability')


%%% Modeling of distrebution of particles
part_diam=[minpad:1:maxpad];           % We assume that particles are
part_N=length(part_diam);              % distributed normally with
part_pdf=normpdf(part_diam,500,200);   % mu=500 and sigma=200
part_cdf=normcdf(part_diam,500,200);
part_cdf(1)=0;
part_cdf(part_N)=1;

figure(2)
subplot(1,2,1)
plot(part_diam,part_pdf)
title('\bf PDF of particles ')
xlabel(' Particle size (micrometers)')
ylabel(' Probability')
subplot(1,2,2)
plot(part_diam,part_cdf)
title('\bf CDF of particles ')
xlabel(' Particle size (micrometers)')
ylabel(' Cumulative probability')


%%% Calculation of big particles size range
minbpad=ceil(minpod/7)+1;
maxbpad=floor(maxpod/3);
bigpart_diam=[minbpad:1:maxbpad];
bigpart_N=length(bigpart_diam);


%%% Calculation of distribution of particles which can move through
%%% this pore system (all movable particles - 100%)
for i=1:part_N
    if minbpad==part_diam(i)
        minbpad_N=i;
    end
end
for i=1:part_N
    if maxbpad==part_diam(i)
        maxbpad_N=i;
    end
end

movable_cdf=part_cdf(1:maxbpad_N)/part_cdf(maxbpad_N);
movable_pdf(1)=movable_cdf(1);

for i=2:length(movable_cdf)
    movable_pdf(i)=movable_cdf(i)-movable_cdf(i-1);
end

bpart_pdf=movable_pdf(minbpad_N:maxbpad_N);  % Distribution of
bpart_cdf=movable_cdf(minbpad_N:maxbpad_N);  % big particles

figure(3)
subplot(1,2,1)
plot(bpart_pdf)
title('\bf PDF of big particles ')
xlabel(' Particle size (micrometers)')
```

```
ylabel(' Probability')
subplot(1,2,2)
plot(bpart_cdf)
title('\bf CDF of big particles ')
xlabel(' Particle size (micrometers)')
ylabel(' Cumulative probability')


%%% Calculation of average length of path of big particles
poresim_N=1000;         % Number of simulation cases for each particle size
for j1=1:bigpart_N
    for i=1:poresim_N
        f1=0;
        path_len(i)=0;  % Length of path of current particle
        while f1==0
            rand1=rand();
            f2=0;
            j2=0;
            while f2==0
                j2=j2+1;
                if rand1<pore_cdf(j2)
                    f2=1;
                end
            end
            curpore_diam=pore_diam(j2);  % Diameter of current pore
            if (bigpart_diam(j1)/curpore_diam)>=(1/3)
                f1=1;                    % Particle stuck in pore
            else
                if (bigpart_diam(j1)/curpore_diam)>(1/7)
                    if (((bigpart_diam(j1)/curpore_diam)-(1/7))/...
                            ((1/3)-(1/7)))<rand()
                        f1=1;            % Particle stuck in pore
                    end
                end
            end
            path_len(i)=path_len(i)+curpore_diam;
        end
    end                                      % Average length for each
    avpath_len(j1)=sum(path_len)/poresim_N;  % particle size (micrometers)
end
avpath_len=avpath_len*(10^(-6));             % (meters)

figure(4)
p21=plot(avpath_len);
title('\bf Average traveling distances of particles')
xlabel('Particle size (micrometers)')
ylabel('Traveling distance (meters)')
set(p21,'Color','blue','LineWidth',2)
aplmin=min(avpath_len);
aplmax=max(avpath_len);
ymax=aplmax+(aplmax-aplmin)/10;
axis([0 bigpart_N 0 ymax])


%%% Calculation of geometry of cylinder model (rw=0.06m)
x_cyl=[0.06:0.01:3.06];
N_cyl=length(x_cyl);

for i=1:N_cyl
```

```
    y_cyl(i)=0.226*(((w*x_cyl(i))/rw)^0.5);
end

dy_cyl=(y_cyl(N_cyl)-y_cyl(1))/10;          % Our model has 10 cells
y10syn_cyl=[y_cyl(1):dy_cyl:y_cyl(N_cyl)];
N10_cyl(1)=1;

for i=2:11
    j=1;
    while y_cyl(j) < y10syn_cyl(i)
        N10_cyl(i)=j;
        j=j+1;
    end
end

for i=1:11
    j=N10_cyl(i);
    x10_cyl(i)=x_cyl(j);    % Calculation of borders of cells
    y10_cyl(i)=y_cyl(j);
end

for i=1:10                                  % Calculation of lengths and
    dx10_cyl(i)=x10_cyl(i+1)-x10_cyl(i);  % average radii of cells
    midy10_cyl(i)=y10_cyl(i)+(y10_cyl(i+1)-y10_cyl(i))/2;
end


%%% Calculation of volume of each cell
for i=1:10
    V(i)=dx10_cyl(i)*3.14*midy10_cyl(i)^2;
end


%%% Creating of arrays with main data
N_steps=floor(tot_time/t_step);   % Number of time steps
fi(1:(N_steps+1),1:10)=fi;            % Array of porosiries
k(1:(N_steps+1),1:10)=k;              % Array of permeabilities


%%% Main loop
for time=1:N_steps     % Loop for each time step
    for cell_N=1:10    % Loop for each cell

        %%% Calculation of chemistry
        veloc=w*fi(time, cell_N)/...     % Velocity of flow in cell
            (3.14*ro_co2*midy10_cyl(cell_N)^2);
        if cell_N==1
            vel1=veloc;
        end
        vel_fact=veloc/vel1;        % Introduction of velocity dependence

        k011=k01*vel_fact;          % Velocity influence
        k021=k02/vel_fact;
        k1=k011*2.7^(-Ea1/(R*T));   % Temperature influence
        k2=k021*2.7^(-Ea2/(R*T));
        r_rate=k1-k2;
        VCaCO3=r_rate*MCaCO3*V(cell_N)*fi(time, cell_N)*t_step/roCaCO3;
```

```
        %%% Calculation of mobilized particles
        Vpart=VCaCO3*Kpart*vel_fact;
        if VCaCO3<0
            Vpart=0;
        end


        %%% Calculation of volume of big particles which moves to next cell
        Vbpart=bpart_pdf*Vpart;        % Volume of mobillized big particles
        mov_Vbpart=(Vbpart.*avpath_len)/dx10_cyl(cell_N);
        mov_Vbpart_tot(cell_N)=sum(mov_Vbpart);  % Volume of big paticles
                                                 % moving to next cell

        %%% Calculation of volume of small particles moving to next cell
        if cell_N>1                          % Volume of mobillized small
            Vspart=Vpart-sum(Vbpart)...      % particles, includic particles
                +mov_Vspart_tot(cell_N-1);  % coming from previous cell
        else
            Vspart=Vpart-sum(Vbpart);
        end

        conc_spart=Vspart/(V(cell_N)*fi(time, cell_N));
        spad=(minbpad-1)/2;           % Average diameter of small perticles
        diff=(1.38*(10^(-23))*T)/... % Diffusivity of small particles
            (3*3.14*visc_co2*spad);
        av_porerad=sum(pore_diam.*pore_pdf)/(2*10^6);
        depos_vol=2*3.14*(diff^(2/3))*... % Volume of deposited particles
            (veloc^(1/3))*conc_spart*(av_porerad^(4/3))*t_step;
        mov_Vspart_tot(cell_N)=Vspart-depos_vol; % Volume of small paticles
                                                 % moving to next cell

        %%% Calculation of new porosities and permeabilities for each cell
        %%% and each time step
        if cell_N>1  % Particles coming from previous cell are included
            fi(time+1, cell_N)=(V(cell_N)*fi(time, cell_N)+VCaCO3+...
                mov_Vbpart_tot(cell_N)+mov_Vspart_tot(cell_N)...
                -mov_Vbpart_tot(cell_N-1)-mov_Vspart_tot(cell_N-1))...
                /V(cell_N);
        else
            fi(time+1, cell_N)=(V(cell_N)*fi(time, cell_N)+VCaCO3+...
                mov_Vbpart_tot(cell_N)+mov_Vspart_tot(cell_N))...
                /V(cell_N);
        end

        k(time+1, cell_N)=k(time+1, cell_N)*((fi(time+1, cell_N)/...
            fi(1,1))^5)*((1-fi(1,1))/(1-fi(time+1, cell_N)))^2;
    end
end

figure(5)
pl31=plot(fi(1,:));
title('\bf Porosity')
xlabel('Cell number')
ylabel('Porosity')
set(pl31,'Color','red','LineWidth',2)
hold on
pl32=plot(fi(N_steps,:));
set(pl32,'Color','blue','LineWidth',2)
fival=[fi(1,1) fi(N_steps,1) fi(1,10) fi(N_steps,10)];
```

```
fimin=min(fival);
fimax=max(fival);
ymin=fimin-(fimax-fimin)/4;
ymax=fimax+(fimax-fimin)/4;
axis([1 10 ymin ymax])
legend('at 1-st time step','at last time step')

figure(6)
pl41=plot(k(1,:));
title('\bf Permeability')
xlabel('Cell number')
ylabel('Permeability, m^2')
set(pl41,'Color','red','LineWidth',2)
hold on
pl42=plot(k(N_steps,:));
set(pl42,'Color','blue','LineWidth',2)
kval=[k(1,1) k(N_steps,1) k(1,10) k(N_steps,10)];
kmin=min(kval);
kmax=max(kval);
ymin=kmin-(kmax-kmin)/4;
ymax=kmax+(kmax-kmin)/4;
axis([1 10 ymin ymax])
legend('at 1-st time step','at last time step')

% Writing results to file formated for Stars
mult_time=t_step:t_step:tot_time;
mult_time=mult_time/(3600*24);
mult_perm(1:N_steps,1:cell_N)=1;
for i=2:(N_steps+1)
    mult_perm(i-1,:)=k(i,:)./k(i-1,:);    % Transmissibility multipliers
end
mult_permrot=flipud(rot90(mult_perm));
mult_t_p=[mult_time; mult_permrot];

mult_file1=fopen('premcyl.txt', 'w');     % File for cylindrical-cone model
fprintf(mult_file1, 'TIME %4.1f\r\n TRANSK KVAR %5.5f %5.5f %5.5f %5.5f %5.5f %5.5f %↙
5.5f %5.5f %5.5f %5.5f\r\n', mult_t_p);
fclose(mult_file1);
mult_file2=fopen('premrad.txt', 'w');     % File for slice-cake model
fprintf(mult_file2, 'TIME %4.1f\r\n TRANSI IVAR %5.5f %5.5f %5.5f %5.5f %5.5f %5.5f %↙
5.5f %5.5f %5.5f %5.5f\r\n', mult_t_p);
fclose(mult_file2);

%%%%%%%%%%%%%%%%%%%%%%%%%%%%%%%%%%%%%%%%%%%%%%%%%%%%%%%%%%%%%%%%%%%%%%%%%%%%%%%
```

APPENDIX B. Data-file for cylindrical-cone model

```
INUNIT SI
WSRF WELL 1
WSRF GRID TIME
WSRF SECTOR TIME
OUTSRF GRID PRES SG SO SW TEMP
OUTSRF WELL LAYER NONE
WPRN GRID 0
OUTPRN GRID NONE
OUTPRN RES NONE
RESULTS XOFFSET          0.0000
RESULTS YOFFSET          0.0000
RESULTS ROTATION         0.0000
RESULTS AXES-DIRECTIONS 1.0 -1.0 1.0

GRID RADIAL 12 4 10 *RW      0
KDIR DOWN
DI CON 0.0365
DJ JVAR         90 90 90 90
DK KVAR  0.09  0.14  0.18  0.23  0.27  0.31  0.35  0.4  0.44  0.59
DTOP           48*1000
POR CON              0.2
PERMI CON          500
PERMJ CON         500
PERMK CON         500
VAMOD 2 0.5 1 0 0.5 *9P 0.5 1
VAMOD 3 0.5 0.5 1 0.5
```

VATYPE ALL

3 1 2 0 0 0 0 0 0 0 0 0

3 1 2 0 0 0 0 0 0 0 0 0

3 1 2 0 0 0 0 0 0 0 0 0

3 1 2 0 0 0 0 0 0 0 0 0

**

3 1 1 2 0 0 0 0 0 0 0 0

3 1 1 2 0 0 0 0 0 0 0 0

3 1 1 2 0 0 0 0 0 0 0 0

3 1 1 2 0 0 0 0 0 0 0 0

**

3 1 1 1 2 0 0 0 0 0 0 0

3 1 1 1 2 0 0 0 0 0 0 0

3 1 1 1 2 0 0 0 0 0 0 0

3 1 1 1 2 0 0 0 0 0 0 0

**

3 1 1 1 1 2 0 0 0 0 0 0

3 1 1 1 1 2 0 0 0 0 0 0

3 1 1 1 1 2 0 0 0 0 0 0

3 1 1 1 1 2 0 0 0 0 0 0

**

3 1 1 1 1 1 2 0 0 0 0 0

3 1 1 1 1 1 2 0 0 0 0 0

3 1 1 1 1 1 2 0 0 0 0 0

3 1 1 1 1 1 2 0 0 0 0 0

**

3 1 1 1 1 1 1 2 0 0 0 0

3 1 1 1 1 1 1 2 0 0 0 0

```
3 1 1 1 1 1 1 2 0 0 0 0
3 1 1 1 1 1 1 2 0 0 0 0
**
3 1 1 1 1 1 1 1 2 0 0 0
3 1 1 1 1 1 1 1 2 0 0 0
3 1 1 1 1 1 1 1 2 0 0 0
3 1 1 1 1 1 1 1 2 0 0 0
**
3 1 1 1 1 1 1 1 1 2 0 0
3 1 1 1 1 1 1 1 1 2 0 0
3 1 1 1 1 1 1 1 1 2 0 0
3 1 1 1 1 1 1 1 1 2 0 0
**
3 1 1 1 1 1 1 1 1 1 2 0
3 1 1 1 1 1 1 1 1 1 2 0
3 1 1 1 1 1 1 1 1 1 2 0
3 1 1 1 1 1 1 1 1 1 2 0
**
3 1 1 1 1 1 1 1 1 1 1 2
3 1 1 1 1 1 1 1 1 1 1 2
3 1 1 1 1 1 1 1 1 1 1 2
3 1 1 1 1 1 1 1 1 1 1 2
END-GRID

MODEL 2 2 2 1
COMPNAME 'Water' 'Soln_Gas'
CMM   0.018 0.048
PCRIT  0 4595.71
```

TCRIT 374.15 31.05

KV1 1.186e+7 8.6212e+8

KV2 0 0

KV3 0 0

KV4 -3816.44 -3103.39

KV5 -227.02 -272.99

PRSR 7120

TEMR 80

PSURF 101

TSURF 16.85

MASSDEN 1050 2

CP 5e-006 9.73459e-007

CT1 0 0.000305715

AVISC 5.48e-14 8.764e-15

BVISC 1515.7 1331.1

VISCTABLE

5	1.51421	0.1165
15	1.13148	0.1174
20	1	0.1177
30	0.79643	0.1338
70	0.404597	0.15
110	0.254635	0.154
150	0.183852	0.16
190	0.145809	0.165
230	0.120485	0.168
270	0.102284	0.172
310	0.0878633	0.175
350	0.0770542	0.179

ROCKFLUID

RPT 1 WATWET

SWT

**	Sw	krw	krow
	0.13	0	0.948
	0.16	0.000939358	0.833203
	0.19	0.00375743	0.725812
	0.22	0.00845422	0.625828
	0.25	0.0150297	0.53325
	0.28	0.0234839	0.448078
	0.31	0.0338169	0.370312
	0.34	0.0460285	0.299953
	0.37	0.0601189	0.237
	0.4	0.076088	0.181453
	0.43	0.0939358	0.133313
	0.46	0.113662	0.0925781
	0.49	0.135268	0.05925
	0.52	0.158751	0.0333281
	0.55	0.184114	0.0148125
	0.58	0.211356	0.00370313
	0.61	0.240476	0
	0.805	0.47555	0
	1	0.79	0

SLT

**	Sl	krg	krog
	0.13	0.2	0
	0.23	0.154194	0

0.33	0.114337	0
0.36875	0.100491	0.00317104
0.4075	0.087539	0.0126842
0.44625	0.0754801	0.0285394
0.485	0.0643144	0.0507367
0.52375	0.054042	0.0792761
0.5625	0.0446628	0.114158
0.60125	0.0361768	0.155381
0.64	0.0285842	0.202947
0.67875	0.0218848	0.256854
0.7175	0.0160786	0.317104
0.75625	0.0111657	0.383696
0.795	0.00714604	0.45663
0.83375	0.00401965	0.535906
0.8725	0.00178651	0.621524
0.91125	0.00044662	0.713485
0.95	0	0.811787
0.975	0	0.878574
1	0	0.948

INITIAL

VERTICAL DEPTH_AVE

INITREGION 1

REFPRES 7120

REFDEPTH 1000

SW CON 0.13

SG CON 0.87

```
NUMERICAL

RUN

DATE 2011 2 1


DTWELL 0.05

**

WELL  'Well-1'

INJECTOR MOBWEIGHT IMPLICIT 'Well-1'

INCOMP  GAS  0.  1.

TINJW  70.

OPERATE  MAX  STG  302.4    **0.007 kg/s

GEOMETRY  K  0.015  0.249  1.  0.

PERF  GEOA  'Well-1'

   1 1 1  1.  OPEN    FLOW-FROM  'SURFACE'


**

WELL  'Well-2'

PRODUCER 'Well-2'

OPERATE  MIN  BHP  7000

GEOMETRY  K  0.015  0.249  1.  0.

PERF  GEOA  'Well-2'

   1 1 10  1.  OPEN    FLOW-TO  'SURFACE'


TIME 36.0

 TRANSK  KVAR  1.01445  1.00476  1.00151  0.99974  0.99842  0.99716  0.99586
0.99447 0.99298 0.99137

TIME 72.0

 TRANSK  KVAR  1.01445  1.00475  1.00150  0.99973  0.99841  0.99714  0.99584
0.99445 0.99295 0.99133
```

TIME 108.0

TRANSK KVAR 1.01446 1.00473 1.00149 0.99972 0.99840 0.99713 0.99582 0.99442 0.99292 0.99130

TIME 144.0

TRANSK KVAR 1.01446 1.00472 1.00148 0.99971 0.99839 0.99712 0.99580 0.99440 0.99289 0.99126

TIME 180.0

TRANSK KVAR 1.01447 1.00471 1.00147 0.99970 0.99838 0.99710 0.99578 0.99438 0.99286 0.99122

TIME 216.0

TRANSK KVAR 1.01447 1.00470 1.00146 0.99969 0.99837 0.99709 0.99577 0.99435 0.99283 0.99118

TIME 252.0

TRANSK KVAR 1.01447 1.00468 1.00145 0.99968 0.99836 0.99707 0.99575 0.99433 0.99280 0.99114

TIME 288.0

TRANSK KVAR 1.01448 1.00467 1.00144 0.99967 0.99835 0.99706 0.99573 0.99431 0.99277 0.99110

TIME 324.0

TRANSK KVAR 1.01448 1.00466 1.00143 0.99966 0.99833 0.99705 0.99571 0.99428 0.99274 0.99107

TIME 360.0

TRANSK KVAR 1.01449 1.00464 1.00142 0.99965 0.99832 0.99703 0.99569 0.99426 0.99271 0.99103

STOP

APPENDIX C. Data-file for slice-cake model

```
INUNIT SI
WSRF WELL 1
WSRF GRID TIME
WSRF SECTOR TIME
OUTSRF GRID PRES SG SO SW TEMP
OUTSRF WELL LAYER NONE
WPRN GRID 0
OUTPRN GRID NONE
OUTPRN RES NONE
RESULTS XOFFSET          0.0000
RESULTS YOFFSET          0.0000
RESULTS ROTATION         0.0000
RESULTS AXES-DIRECTIONS 1.0 -1.0 1.0

GRID RADIAL 10 1 5
KDIR DOWN
DI CON 0.3
DJ CON             9.24
DK ALL         50*0.2
DTOP           10*1000
POR CON             0.2
PERMI CON          500
PERMJ CON          500
PERMK CON          500
END-GRID
```

MODEL 2 2 2 1

COMPNAME 'Water' 'Soln_Gas'

CMM 0.018 0.048

PCRIT 0 4595.71

TCRIT 374.15 31.05

KV1 1.186e+7 8.6212e+8

KV2 0 0

KV3 0 0

KV4 -3816.44 -3103.39

KV5 -227.02 -272.99

PRSR 7120

TEMR 80

PSURF 101

TSURF 16.85

MASSDEN 1050 2

CP 5e-006 9.73459e-007

CT1 0 0.000305715

AVISC 5.48e-14 8.764e-15

BVISC 1515.7 1331.1

VISCTABLE

5	1.51421	0.1165
15	1.13148	0.1174
20	1	0.1177
30	0.79643	0.1338
70	0.404597	0.15
110	0.254635	0.154
150	0.183852	0.16
190	0.145809	0.165

230	0.120485	0.168
270	0.102284	0.172
310	0.0878633	0.175
350	0.0770542	0.179

ROCKFLUID

RPT 1 WATWET

SWT

** Sw	krw	krow
0.13	0	0.948
0.16	0.000939358	0.833203
0.19	0.00375743	0.725812
0.22	0.00845422	0.625828
0.25	0.0150297	0.53325
0.28	0.0234839	0.448078
0.31	0.0338169	0.370312
0.34	0.0460285	0.299953
0.37	0.0601189	0.237
0.4	0.076088	0.181453
0.43	0.0939358	0.133313
0.46	0.113662	0.0925781
0.49	0.135268	0.05925
0.52	0.158751	0.0333281
0.55	0.184114	0.0148125
0.58	0.211356	0.00370313
0.61	0.240476	0
0.805	0.47555	0
1	0.79	0

SLT

** Sl	krg	krog
0.13	0.2	0
0.23	0.154194	0
0.33	0.114337	0
0.36875	0.100491	0.00317104
0.4075	0.087539	0.0126842
0.44625	0.0754801	0.0285394
0.485	0.0643144	0.0507367
0.52375	0.054042	0.0792761
0.5625	0.0446628	0.114158
0.60125	0.0361768	0.155381
0.64	0.0285842	0.202947
0.67875	0.0218848	0.256854
0.7175	0.0160786	0.317104
0.75625	0.0111657	0.383696
0.795	0.00714604	0.45663
0.83375	0.00401965	0.535906
0.8725	0.00178651	0.621524
0.91125	0.00044662	0.713485
0.95	0	0.811787
0.975	0	0.878574
1	0	0.948

INITIAL

VERTICAL DEPTH_AVE

INITREGION 1

REFPRES 7120

```
REFDEPTH 1000
SW CON 0.13
SG CON 0.87

NUMERICAL
RUN
DATE 2011 2 1

DTWELL 0.05
**
WELL  'Well-1'
INJECTOR MOBWEIGHT IMPLICIT 'Well-1'
INCOMP  GAS  0.  1.
TINJW  70.
OPERATE  MAX  STG  302.4    **0.007 kg/s
GEOMETRY  K  0.015  0.249  1.  0.
PERF  GEOA  'Well-1'
   1 1 1  1.  OPEN    FLOW-FROM  'SURFACE'

**
WELL  'Well-2'
PRODUCER 'Well-2'
OPERATE  MIN  BHP  7000
GEOMETRY  K  0.015  0.249  1.  0.
PERF  GEOA  'Well-2'
   1 1 10  1.  OPEN    FLOW-TO  'SURFACE'

TIME 36.0
```

TRANSI IVAR 1.01445 1.00476 1.00151 0.99974 0.99842 0.99716 0.99586 0.99447 0.99298 0.99137

TIME 72.0

TRANSI IVAR 1.01445 1.00475 1.00150 0.99973 0.99841 0.99714 0.99584 0.99445 0.99295 0.99133

TIME 108.0

TRANSI IVAR 1.01446 1.00473 1.00149 0.99972 0.99840 0.99713 0.99582 0.99442 0.99292 0.99130

TIME 144.0

TRANSI IVAR 1.01446 1.00472 1.00148 0.99971 0.99839 0.99712 0.99580 0.99440 0.99289 0.99126

TIME 180.0

TRANSI IVAR 1.01447 1.00471 1.00147 0.99970 0.99838 0.99710 0.99578 0.99438 0.99286 0.99122

TIME 216.0

TRANSI IVAR 1.01447 1.00470 1.00146 0.99969 0.99837 0.99709 0.99577 0.99435 0.99283 0.99118

TIME 252.0

TRANSI IVAR 1.01447 1.00468 1.00145 0.99968 0.99836 0.99707 0.99575 0.99433 0.99280 0.99114

TIME 288.0

TRANSI IVAR 1.01448 1.00467 1.00144 0.99967 0.99835 0.99706 0.99573 0.99431 0.99277 0.99110

TIME 324.0

TRANSI IVAR 1.01448 1.00466 1.00143 0.99966 0.99833 0.99705 0.99571 0.99428 0.99274 0.99107

TIME 360.0

TRANSI IVAR 1.01449 1.00464 1.00142 0.99965 0.99832 0.99703 0.99569 0.99426 0.99271 0.99103

STOP